

## Response to Reviewer #1

Dear Anonymous Referee #1:

Thank you for reviewing our manuscript. We have carefully considered all your comments and revised the manuscript accordingly. In particular, we appreciate your suggestion to add details about the selection of the reference DEM and filtering method of the dh values. We have reprocessed all the DEM data (1) taking the penetration of SRTM DEM over the snow and ice area into consideration and (2) using new outlier-filtering standard. Also, we have added two new figures depicting annual and monthly glacial velocities of different points along centerline of the western branch.

Here, we respond (in black plain text) to your comments (in blue italics) one by one. We also attach a marked-up version of the revised manuscript and supplementary information.

Best regards,

Mingyang Lv, Guanyu Li and other co-authors

*L54: The GLOF was in 2015. Check the reference. It is from 2014.*

Response: Thanks for this suggestion. The GLOF early warning system was implemented between 2011 and 2013 (hence the reference of Haemmig et al., 2014), and a GLOF occurred in June 2015 while the early warning station was submerged due to the rapid impoundment of the glacial lake (Round et al., 2017). Therefore, we have added another reference (Round et al., 2017) to the sentence here.

*L58: Why was the risk high? More information would be nice*

Response: Thank you for pointing this out. Written in Round et al. (2017), in the period following 2016, 'GLOF hazard potential is expected to remain high for a number of years as the still slightly elevated tongue velocity continues to transport mass to the terminus area, potentially increasing the height of the ice dam until mass transport to the terminus area falls below the ablation rate'. Accordingly, we have added additional information after the sentence in L58. The text now reads 'They also suggested that the potential for further GLOFs in the period following 2016 was high, as the glacier tongue continued to supply mass to the terminus area, maintaining the height of the existing ice dam.'

*L59: How did they figure it out that there were some surges before 2000?*

Response: Thanks for picking this up, we have added more information to the manuscript.

Haemmig et al. (2014) and Round et al. (2017) found that peak volumes of GLOF in 1978 and 1999 coincide with periods of suspected advance or thickening. They speculated that the clustering of peak flood volumes between late 1990s and early 2000s might indicate a glacier surge prior to 2000. Zhang et al. (2022) found the glacial velocities peaked (surge events) with glacier surface characteristics change in 1975-1978 and 1995-1997 respectively, using historic Landsat imageries and glacial velocity data. Bhambri et al. (2019) also reported one of the surges lasted from 1994 to 1997.

We have changed the original text to 'They speculated that the recurring GLOFs recorded in 1978 and 1999 could indicate the maximum return period of glacier surges. Bhambri et al. (2019) reported one of the surge events lasted from 1994 to 1997. Another former surge from 1975 to 1978 was confirmed by Zhang et al. (2022) using glacial velocity data derived from Landsat images, again indicating an approximate surge cycle of 19-20 years.'

*L62: replace "surface conditions" with "parameters"*

Response: Thanks for this suggestion. We've changed it accordingly.

*L63: replace "mass balances" with "surface elevation changes"*

Response: Thanks for this suggestion. We've changed it in the new text.

*L78: please provide a reference for "polythermal"*

Response: Thanks for this suggestion. We cited Shi and Liu (2000) in this sentence. According to Shi and Liu (2000), glaciers on the northern slope of mid to western Himalayas and Karakoram are polythermal ones.

*L143: Which areas did you use for the coregistration? All or only off-glacier? Please clarify*

Response: Thank you for pointing this out. We have co-registered the ASTER DEMs and HMA DEMs to the reference SRTM DEM using Demcoreg (Shean et al., 2016). All ASTER DEMs and HMA DEMs covering Kyagar glacier were used for co-registration, including glacier area and off-glacier area. During the process of the Demcoreg software, RGI V6.0 data is used to generate glacier

polygon raster mask for input DEMs, thus technically only off-glacier areas will affect co-registration results.

In the new manuscript, it reads 'Demcoreg is a collection of Python and shell scripts for co-registration of DEMs, which automatically implements the correction algorithm using areas of stable terrain, where the DEMs are least error-prone (Berthier et al., 2016).'

*\*L146: Why did you compute the elevation difference relative to SRTM? SRTM is affected by SAR signal penetration. Why don't you use a ASTER DEM from 2000 as a reference? This would reduce the bias. Moreover, SRTM has considerable voids in HMA, filled with other DEM data like ASTER GDEM2. This can lead to some biases in the elevation changes and thus in the subsequent analyses by using e.g. BEAST or PWLF. You should provide information on which areas of the SRTM DEM were filled by other elevation data.*

Response:

Thank you for this suggestion.

1. Suffering from heavy cloud and snow cover, and the rough mountainous topography, individual ASTER DEMs are usually of poor quality and cannot be trusted. ASTER DEMs would not be suitable as a reference for co-registration. Although SRTM is affected by SAR signal penetration, there are many researches and applications using SRTM to calculate glacier mass balance, given its higher precision and well-defined timestamp (Berthier et al., 2016; Lv et al., 2020).

2. Following your suggestion, we are aware that SRTM Non-Void Filled (Digital Object Identifier (DOI) number: /10.5066/F7K072R7) elevation data is more suitable as a reference DEM in our study. As shown in the figure below (Fig. R1), the percentage of void pixels over Kyagar Glacier in SRTM Non-Void Filled data is less than 9%, while most of them are located at the highest elevations. The area below 5600 m affected by the surge contains very few void pixels.

3. Given the known penetration of C-band radar waves over snow and glacier-covered terrain (Gardelle et al, 2013), the SRTM Non-Void Filled data was modified based on the identification of snow- and ice-facies, following previous study in the nearby region. The related text in Section 3.1.3 is now 'In order to correct for surface penetration, we applied adjustments of +5.5 m over firn and snow areas and +1.1 m over clean ice areas following previous studies in the

nearby region (e.g. Lv et al., 2020a). Identification of ice and snow facies is based on a Landsat ETM+ image acquired in February 2000 which was approximately coincident with the SRTM mission'.

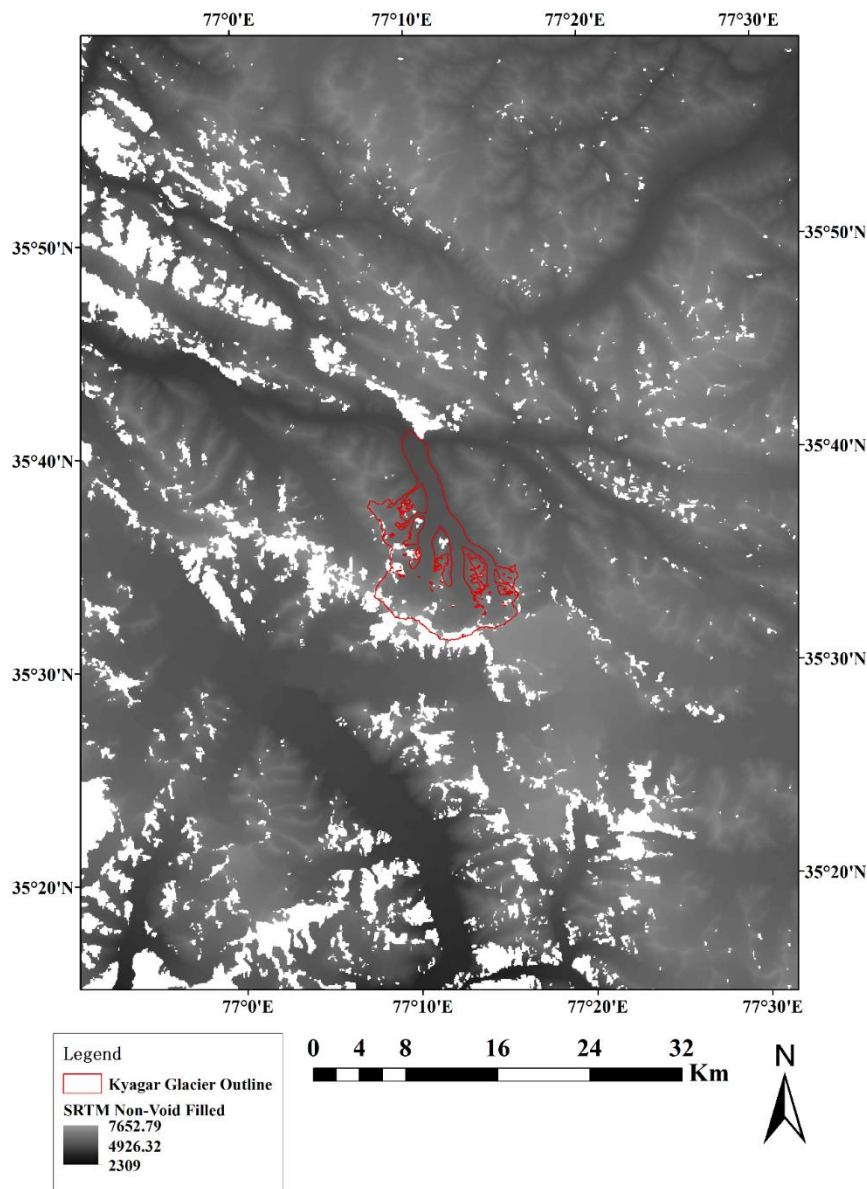


**Figure R1: The distribution of void pixels for Kyagar Glacier and its adjacent area in SRTM Non-Void Filled data**

4. Using the resampled non-void filled and penetration-corrected SRTM DEM as the new reference DEM, DEM co-registration, outlier filtering and post-processing of DEM differencing data were totally reprocessed. Parameter maps quantifying elevation changes of Kyagar Glacier in related figures were updated, as well as elevation-change rates data in Section 4.1. Meanwhile, we provide a new version of mean differences and the standard deviation (SD) before and

after co-registration process in the supplement (Table S1). All the updated results are in good agreement with the previous results.

*\*L152: You should apply a filter that accounts for the time difference relative to your reference DEM. e.g. for a DEM in 2010, the filter should be +/-30 m. Same for the filter for areas below 5600 m.*

Response: Thank you for this suggestion. As you suggested, for the pixels above 5600 m a.s.l., we applied a threshold that varied with time interval of different DEMs. The surface elevation changes below 5600 m a.s.l. could be highly affected by the glacier surge, especially over the terminus area of the Kyagar glacier. Thus, pixels below 5600 m a.s.l. were filtered with a threshold of  $\pm 150$  m to avoid excluding any real values associated with the surge event. Even though some outliers might still exist after the filtering, they could hardly affect the final result, as the DEM post-processing would probably rule them out.

We used these new outlier-free elevation-change maps for further processing.

*L214ff: It is hard to obtain the temporal evolution from the plot in Figures 5 and 6. It would be helpful if you could provide a plot of the velocity measured at the same spots as for the elevation changes (Fig. 4), or even more spots to better evaluate the temporal evolution of the velocities, in particular the monthly evolution.*

Response: Thank you for this constructive suggestion. According to Figure 5 and 6 (Figure 7 in the new manuscript), we have selected six points along the centerline of west branch (2, 4, 6, 8, 10, 12 km from the terminus in Fig. R2) to show their annual and monthly velocities (Fig. R3 & R4). These figures and related information have been added to the manuscript.

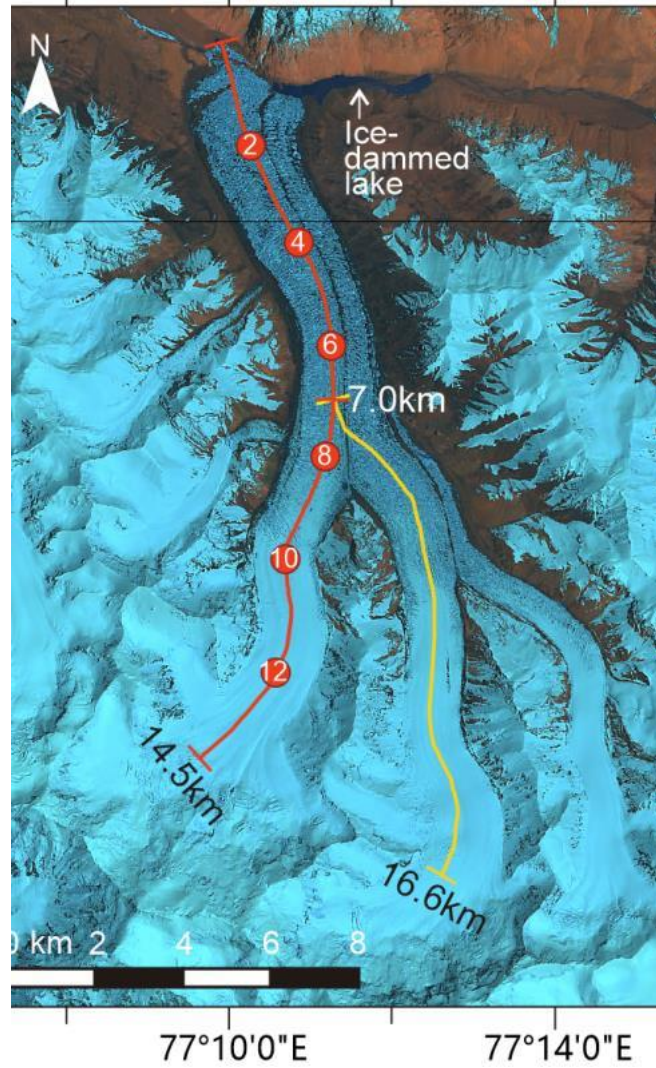


**Figure R2: The points we selected along the western branch which is 2, 4, 6, 8, 10 ,12 km from the terminus respectively.**

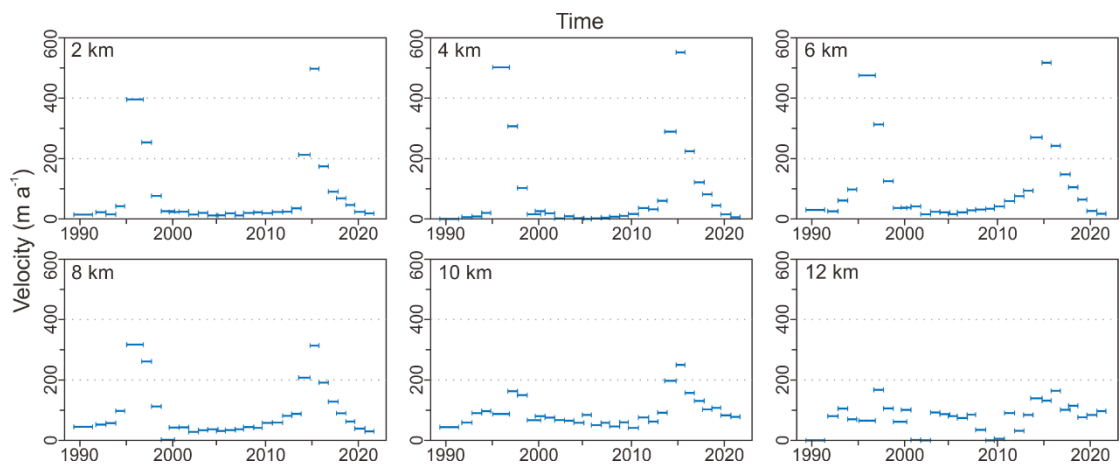


**Figure R3: Annual velocities of different points along the western branch of Kyagar Glacier from 1989 to 2021. The points are selected at 2, 4, 6, 8, 10 ,12 km from the terminus.**

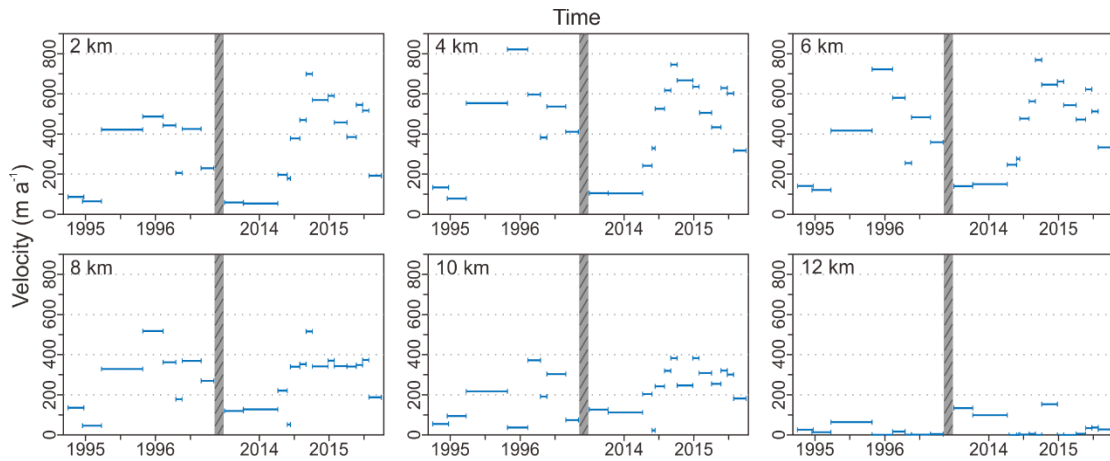


**Figure R4: Near monthly velocities of different points along the western branch of Kyagar Glacier during two surging periods. The points are selected at 2, 4, 6, 8, 10, 12 km from the terminus.**

*L230: Any explanation why this area did not show any signal?*

Response: Thanks for pointing this out. As shown in Fig. 7 and Fig. 8 (Fig. 9 and Fig. 10 in new manuscript), the elevation change over 4-7 km before and after the surge was much smaller than those of regions over 0-4 km and 7-10 km. Combined with the relatively poor quality of the DEMs we used, especially the ASTER DEMs, very few abnormal change points could be detected by the BEAST and PWLF model over 4-7 km. With better quality DEMs and finer temporal coverage, a clear change signal could also be detected over 4-7 km, even though the signal might be small.

We added a sentence at the end of this paragraph 'This unclear change signal could result from the limited quality of the DEMs at this time'.

*L242: Annual GLOF? You are talking about a single event. If not please provide more information.*

Response: Thank you for this suggestion. We are talking about annual lake outbursts from 1996 to 2009 here. We have changed the original text to 'After reaching its maximum area in each year, the lake discharged almost entirely within about two days, likely resulting in annual GLOFs to the downstream valley from 1996 to 2009'.

*L243: A graph showing the temporal evolution of the lake area (time vs. lake area) would be helpful to illustrate the variations in the lake area.*

Response: We investigated the evolution of the ice-dammed lake using visual interpretation of satellite images and the SRTM DEM (Fig. S1-S11). Meanwhile, we also provide a graph showing the temporal evolution of the lake area and surface elevation in Fig. 9, which is now Fig. 11 in the new manuscript.

*L245: what do you mean by historic? Which period?*

Response: Sorry for the misleading sentence. We have changed the original sentence into two sentences which are now written as 'In contrast to the earlier period, the lake did not fully disappear during each drainage event. The timing of each reduction in lake area suggests historic lake outbursts took place during every summer since 1996 (July to September).'

*L252: "At the beginning of the surge...." when? Please provide a date information*

Response: Thanks for this suggestion. As shown in Fig. 5e, velocities along the glacier surface 2-4 km from the terminus started to increase slightly since October 2012, which can be considered as the buildup phase before the glacier surge. We have changed the original sentence to 'At the beginning of the surge, velocities increased uniformly and slowly along the glacier tongue since October 2012 (Fig. 5e, 6)' as an independent sentence.

*L254: You mention in the previous sentence that no surge front was formed. And now, you are talking about a surge front. Please clarify*

Response: Sorry for the clumsy expression. We have changed the original sentence "... with no obvious surge front forming until April 2014 (Fig. 5e,6a)" to "It was not until April 2014 that an obvious surge front formed (Fig. 7a), ...".

*L255: How did you figure out that there was compression?*

Response: Thanks for this suggestion. For the 3-4 km region, the velocity didn't change obviously from November 2011 to November 2013, while  $T_s$  values in 2012 and 2013 were detected. Thus, we suggest that a notable surface elevation increase in 2012 and 2013 over 3-4 km resulted from a compression of ice that could not be transported further downglacier.

In order to clearly express the compression, we have changed the original sentence 'There was a zone of intense compression 3-4 km from the terminus resulting in a notable elevation increase. Consequently,  $T_s$  values in 2012 and 2013 were detected over the middle part of the receiving zone (Fig. 8d), while elevations over the reservoir zone had no obvious change during this period

(Fig. 10)' to ' $T_s$  values in 2012 and 2013 were detected over the area 3-4 km from the terminus (Fig. 10d), indicating a notable elevation increase, which we speculate resulted from intense compression of ice that could not be transported into the middle part of the receiving zone, while elevations over the reservoir zone had no obvious change during this period (Fig. 12)'.

*L280: which profile? Unclear sentence. Please rephrase this explanation.*

Response: Thanks for pointing this out. We identified the last profile with a decreasing velocity after the peak profile as the surge termination, even though the reduction may be small (e.g.  $<10 \text{ m a}^{-1}$ ), and this profile is 2019/08-2020/09 profile in Fig. 5f. Now we have changed the original sentence to 'the lattermost profile (2019/08-2020/09 in Fig. 5f)'.

*L302: Why does BEAST contain more information? Please explain*

Response: Thanks for the comment. Compared to the PWLF process, BEAST model was the first step processing the time-series DEMs, which made  $R^2$  and standard deviation calculated by BEAST contain more information about raw data quality and spatial-temporal distribution. Now we have changed the explanation to ' $R^2$  in PWLF is higher than that in BEAST, while the standard deviation in PWLF is less than that in BEAST. On the other hand, as the BEAST model is firstly conducted to process the time-series DEMs, the results of BEAST could contain more information about raw data quality and spatial-temporal distribution'.

*L307: Please introduce high abnormal change probability and add a cross-link to the respective figure*

Response: Thank you for this suggestion.

1. BEAST model can estimate many parameters of time series data, such as probability of being a changepoint, number of changepoints, probability distribution of total changepoint number (Zhao et al., 2019). BEAST model gives not only a probability distribution of having a changepoint in the trend at each point of time (named as cpOccPr), but also the probabilities associated with the changepoints (named as cpPr). Changepoint is at last identified by the cpPr value, which is calculated by a sum-filtering to the cpOccPr curve. Now we have added the summed cpPr values in the new version Figure 4b,e,h,k. We add the necessary explanation text in Section 3.3 as 'The abnormal changes in an time-series elevation data were identified by the probability

parameters, which are calculated by summing the probability distribution in the trend signals (Fig. 4b,e,h,k)'.

2. The IPCC Likelihood Scale indicates an event is 'more likely than not' to occur when the probability of occurrence is greater than 0.50, 'likely' with probabilities above greater than 0.66, 'very likely' with probabilities above 0.9 and 'virtually certain' when the probability is above 0.99, as shown in Table R1 (Mastrandrea et al., 2010). Thus, we set probability  $\geq 0.5$  as the threshold to find the changepoints which is more likely than not to occur in this research. We consider that the pixels with probability value large than 0.50 are high enough as possible abnormal change points. Now we have added these information and reference in Section 3.3 as 'According to IPCC Likelihood Scale, the abnormal elevation change is 'more likely than not' to occur when the probability is greater than 0.50 (Mastrandrea et al., 2010). Therefore, we suggest the pixels with probability value larger than 0.50 are credible enough to be considered as abnormal changes'.

**Table R1: Confidence and Likelihood in the IPCC Fifth Assessment Report  
FACT SHEET**

Term	Likelihood of the outcome
Virtually certain	>99% probability
Extremely likely	>95% probability
Very likely	>90% probability
Likely	>66% probability
More likely than not	>50% probability
About as likely as not	33 to 66% probability
Unlikely	<33% probability
Extremely unlikely	<5% probability
Exceptionally unlikely	<1% probability

*L313: You should also mention that a large amount of DEMs is needed to apply this approach. This might be a limiting factor.*

Response: Thanks for the suggestion. We have added "The only limiting factor for applying this approach would be that a large amount of DEMs with good spatial and temporal coverage are needed." at the end of this paragraph.

## Reference

- Berthier, E., Cabot, V., Vincent, C., and Six, D.: Decadal Region-Wide and Glacier-Wide Mass Balances Derived from Multi-Temporal ASTER Satellite Digital Elevation Models. Validation over the Mont-Blanc Area, *Frontiers in Earth Science*, 4, <https://doi.org/10.3389/feart.2016.00063>, 2016.
- Bhambri, R., Hewitt, K., Kawishwar, P., Kumar, A., Verma, A., Snehmani, Tiwari, S., and Misra, A.: Ice-dams, outburst floods, and movement heterogeneity of glaciers, Karakoram, *Global and Planetary Change*, 180, 100-116, <https://doi.org/10.1016/j.gloplacha.2019.05.004>, 2019.
- Gardelle, J., Berthier, E., Arnaud, Y., and Käab, A.: Region-wide glacier mass balances over the Pamir-Karakoram-Himalaya during 1999-2011, *The Cryosphere*, 7(4), 1263-1286, <https://doi.org/10.5194/tc-7-1263-2013>, 2013.
- Haemmig, C., Huss, M., Keusen, H., Hess, J., Wegmüller, U., Ao, Z., and Kulubayi, W.: Hazard assessment of glacial lake outburst floods from Kyagar glacier, Karakoram mountains, China, *Ann. Glaciol.*, 55(66), 34-44, <https://doi.org/10.3189/2014AoG66A001>, 2014.
- Lv, M., Quincey, D. J., Guo, H., King, O., Liu, G., Yan, S., Lu, X., and Ruan, Z.: Examining geodetic glacier mass balance in the eastern Pamir transition zone, *J. Glaciol.*, 1-11, <https://doi.org/10.1017/jog.2020.54>, 2020.
- Mastrandrea, M. D., Field, C. B., Stocker, T. F., Edenhofer, O., Ebi, K. L., Frame, D. J., Held, H., Kriegler, E., Mach, K. J., and Matschoss, P. R.: Guidance note for lead authors of the IPCC fifth assessment report on consistent treatment of uncertainties, 2010.
- Round, V., Leinss, S., Huss, M., Haemmig, C., and Hajsek, I.: Surge dynamics and lake outbursts of Kyagar Glacier, Karakoram, *The Cryosphere*, 11(2), 723-739, <https://doi.org/10.5194/tc-11-723-2017>, 2017.
- Shean, D. E., Alexandrov, O., Moratto, Z. M., Smith, B. E., Joughin, I. R., Porter, C., and Morin, P.: An automated, open-source pipeline for mass production of digital elevation models (DEMs) from very-high-resolution commercial stereo satellite imagery, *ISPRS J. Photogramm. Remote Sens.*, 116, 101-117, <https://doi.org/10.1016/j.isprsjprs.2016.03.012>, 2016.
- Shi, Y. and Liu, S.: Estimation on the response of glaciers in China to the global warming in the 21st century, *Chinese Science Bulletin*, 45, 668-672, <https://doi.org/10.1007/BF02886048>, 2000.
- Zhang, M., Chen, F., Tian, B., Liang, D., and Yang, A.: Characterization of Kyagar Glacier and Lake Outburst Floods in 2018 Based on Time-Series Sentinel-1A Data, *Water*, 12(1), <https://doi.org/10.3390/w12010184>, 2020.
- Zhang, Z., Zhao, J., Liu, S., Zhang, Q., Jiang, Z., Xu, Y., and Hu, K.: Characterization of Three Surges of the Kyagar Glacier, Karakoram, SSRN, <http://dx.doi.org/10.2139/ssrn.4065221>, 2022.
- Zhao, K., Wulder, M. A., Hu, T., Bright, R., Wu, Q., Qin, H., Li, Y., Toman, E., Mallick, B., Zhang, X., and Brown, M.: Detecting change-point, trend, and seasonality in satellite time series data to track abrupt changes and nonlinear dynamics: A Bayesian ensemble algorithm, *Remote Sens. Environ.*, 232, 111181, <https://doi.org/10.1016/j.rse.2019.04.034>, 2019.

## Response to Prof. Rakesh Bhambri

Dear Prof. Rakesh Bhambri,

Thank you for your time reviewing our manuscript. Your valuable comments are very helpful in improving the content. We have adjusted the manuscript accordingly, including adding some further references and making changes to related sentences and figures as you suggested. In particular, we appreciate your suggestion of adding detailed descriptions of how we extracted the lake area and elevation.

We respond (in black plain text) to all your comments (in blue italics) in-turn, and attach a marked-up version of the revised manuscript and supplement, combined with the changes suggested by our second reviewer.

Best regards,

Mingyang Lv, Guanyu Li, and other co-authors

*This study presented a detailed study of surges of Kyagar Glacier and associated ice-dammed outburst burst floods using a time series of Landsat satellite imagery and ASTER digital elevation models. The manuscript is well-written and nicely structured, and I have given a few minor suggestions for improvement.*

*In the introduction, there is a need to highlight gap areas in previous studies.*

Response: Thanks for the constructive suggestion. We have added necessary information at the end of Paragraph 4 in the Introduction Section to highlight research gaps. It now reads ‘... Like other glacier surge studies utilizing remote sensing, most of them primarily focused on the evolution of surface velocity and description of related surface features, with limited DEMs used to discuss the amplitude of surface elevation change caused by the surges and analyse mass balance conditions.’.

*L21: ‘from’ 2000 to 2001.*

Response: Thanks for this suggestion. We’ve added ‘from’ here.

*L23: data’sets’.*

Response: Thanks for this suggestion. We’ve changed accordingly.

*L25: Seasonal variations in 'surface' flow.*

Response: Thanks for this suggestion. We've changed it in the new text.

*L26: Surge activity 'of Kyagar'*

Response: Accepted and changed.

*L29-75: Please refer basic papers on Surge glaciers in the introduction (Jiskoot 2011; Truffer et al. 2021).*

Response: Thanks for listing these helpful references. We have cited Jiskoot (2011) and Truffer et al. (2021) in the first paragraph of the Introduction.

*L35: "The Karakoram is one such zone (Guillet et al., 2022; Sevestre and Benn, 2015)."  
You can merge a very small sentence with the previous or later sentence.*

Response: Thanks for this suggestion. We have changed the original sentence to "Sometimes, climate conditions, topographic and geologic features can intensify such imbalances, and the Karakoram is one such zone (Guillet et al., 2022; Sevestre and Benn, 2015)."

*L40: You can replace Bhambri et al. (2017) with Bhambri et al. (2019), as the previous reference is related to only the surging process. In contrast, the 2019 reference is based on GLOFs events associated with Surging glaciers.*

Response: Thank you for this suggestion. We've replaced Bhambri et al. (2017) with Bhambri et al. (2019) in this sentence. We still cite Bhambri et al. (2017) in other sentences as we believe it is also supportive to the Introduction Section.

*L56: over previous surge events. You can refer more references (Haemmig et al., 2014; Bhambri et al., 2019).*

Response: Thank you and we have cited Haemmig et al. (2014) and Bhambri et al. (2019) in this sentence.

*L60: Bhambri et al. (2019) also reported a 1990s surge from 1994 to 1997 (Fig 3). You may mention it here.*

Response: Thanks for your suggestion. We have changed the original text to ‘... They speculated that the recurring GLOFs recorded in 1978 and 1999 could indicate the maximum return period of glacier surges. Bhambri et al. (2019) reported one of the surge events lasted from 1994 to 1997. Another former surge from 1975 to 1978 was confirmed by Zhang et al. (2022) using glacial velocity data derived from Landsat images, again indicating an approximate surge cycle of 19-20 years. ...’.

*L66: “Kyagar Glacier is an ideal case on which to test a new approach for describing glacier surge events using DEMs generated from ASTER images”. Bhambri et al. (2019) also used time series (10 DEMs) of ASTER DEMs to understand the evolution of surge (Supplementary Fig. S6). However, your study used a large number of ASTER DEMs, and you may highlight this here.*

Response: Thanks for this suggestion. We have cited Bhambri et al. (2019) in this sentence, and we add extra sentences to highlight the difference of our study at the end of this paragraph. ‘As well as using an overall larger number of DEMs to reconstruct the surging process than previous studies (Pitte et al., 2016; Bhambri et al., 2019), we also applied HMA DEMs for the first time to better understand the evolution of the Kyagar Glacier surge.’

*L66: “Kyagar Glacier is an ideal case on which to test a new approach for describing glacier surge events using DEMs generated from ASTER images”. You may refer here Pitte et al. (2016), possibly the first used time series of ASTER DEMs for glacier surge study.*

Response: Thank you for mentioning this valuable study. We have cited Pitte et al. (2016) in this sentence.

*L69: the best of our knowledge, no earlier study used HMA DEMs for understanding the evolution of the Kyagar Glacier surge, and you may highlight this here.*

Response: Thanks for this suggestion. We’ve added this information to the end of this paragraph reading ‘As well as using an overall larger number of DEMs to reconstruct the surging process than previous studies (Pitte et al., 2016; Bhambri et al., 2019), we also applied HMA DEMs for the first time to better understand the evolution of the Kyagar Glacier surge.’.

*L83: You may replace Bolch et al. (2012) with Bookhagen and Burbank (2006) and Thayyen, and Gergan (2010).*

Response: Thank you for this suggestion. We've removed Bolch et al. (2012) in the Reference, and add Bookhagen and Burbank (2006) and Thayyen and Gergan (2010) here.

*L93: ice crevasses and "ice pinnacles" (old 1920s field photographs show this).*

Response: Thanks for your suggestion. We've added 'ice pinnacles' in the new text.

*L148-149: "Non-glacier pixels with values greater than 3 standard deviations from the mean were discarded (Ragettli et al., 2016), and the vertical offsets of most selected ASTER/ HMA DEMs relative to SRTM over stable terrain were reduced to within  $\pm 2$  m." Non-glacier pixels and stable terrain are mentioned in this sentence. Are Non-glacier pixels not containing stable terrain pixels? Please check.*

Response: Sorry for the misleading sentence. The definition of non-glacier pixels and stable terrain are the same in our DEM co-registration and outlier filtering processing. We've changed the 'stable terrain' to 'non-glacierised terrain'.

*L184: Landsat 7. You can shift lines 191-192 on SLC here and link with this sentence.*

Response: Thanks for this suggestion. We've shifted the sentence accordingly. The text now reads 'Panchromatic bands of Landsat-7 and Landsat-8 with a resolution of 15 m were selected as the potential image pairs between 1999 and 2021. Despite the Scan Line Corrector failure in May 2003 (Markham et al., 2004), we found that feature tracking of Landsat-7 image pairs from 2003 to 2013 was still viable for tracking features between the data gaps.'

*L204: You may replace one with the first surge and the other with the second surge.*

Response: Thanks for this suggestion. We've changed the original sentence to 'The first surge occurred from 1992 to 1998 and the second surge from 2012 to 2019'.

*L238-239: “We investigated the evolution of the ice-dammed lake using visual interpretation of satellite images and the SRTM DEM (Fig. S1-S11).” You can shift this line in the method part.*

Response: Thanks for this suggestion. We add a new Section 3.6 ‘Visual interpretation of ice-dammed lake evolution’ in the method part, and shifted line 238-239 to it. According to the suggestion from Anonymous Referee #1, we replaced original reference 1-arc SRTM data with 3-arc SRTM Non-Void Filled data, which is not good enough for extracting surface elevation of the ice-dammed lake. Therefore, we used HMA DEM on 13 January 2013, when the lake area fully disappeared, as the reference DEM for estimating ice-dammed lake surface elevation. We found that the updated elevation results are in good agreement with our previous results.

The text in Section 3.6 now reads as below:

‘We investigated the area of the ice-dammed lake using visual interpretation of satellite images. 148 Landsat images were selected and manually digitised to extract near-monthly lake boundaries (Fig. S1-S11). The HMA DEM obtained on 13 January 2013, when the lake was completely discharged, was taken as reference DEM. We assume the lake bed remained stable during the studied period, and the lake surface elevations at different times were then estimated using the extracted lake boundaries and the reference HMA DEM.’

*Fig 1: Some north-facing glaciers do not contribute to Kaygar glacier ice-dammed lake. Please carefully check.*

Response: Thank you for pointing this out. As shown in the figure below (Fig. R1), The upstream basin of the ice-dammed lake was calculated by ArcGIS hydrology tools. Figure R1 shows that some glaciers in the northern part of the basin have tributaries flowing to the north and south respectively, and the southern tributary contributes to the lake. The glacial boundaries are directly from RGI 6.0, thus we did not manually remove the northern tributaries from the glaciers.

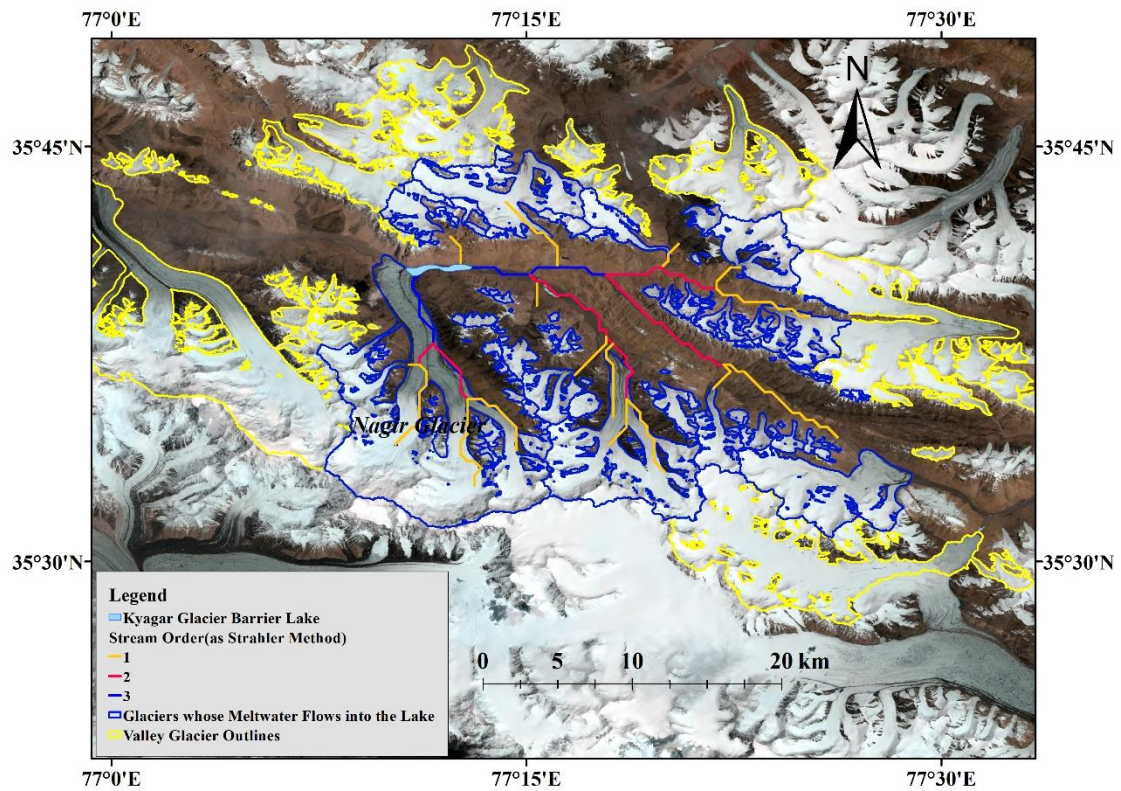


**Figure R1: The upstream basin of Kyagar Glacier ice-dammed lake**

*Fig 2: In this figure, you may mark the western and eastern branches.*

Response: Thanks for this suggestion. We've marked the western and central branches of Kyagar Glacier in the new Figure 2.

*Fig 5 and 6: The legend of this fig may be improved, and image pair information may be present in the same line.*

Response: Thank you for this suggestion. We've improved the legend of related figures to make them clearer to readers.

*Fig 7: You may also add non-glacier elevation change in this fig which will present the accuracy of elevation change at the non-glacier area.*

Response: Thanks for this suggestion. We've added non-glacier elevation change in Figure 7 (Figure 9 in the new manuscript) accordingly.

## Reference

- Bhambri, R., Hewitt, K., Kawishwar, P., Kumar, A., Verma, A., Snehmami, Tiwari, S., and Misra, A.: Ice-dams, outburst floods, and movement heterogeneity of glaciers, Karakoram, *Global and Planetary Change*, 180, 100-116, <https://doi.org/10.1016/j.gloplacha.2019.05.004>, 2019.
- Bolch, T., Pieczonka, T., and Benn, D. I.: Multi-decadal mass loss of glaciers in the Everest area (Nepal Himalaya) derived from stereo imagery, *The Cryosphere*, 5(2), 349-358, <https://doi.org/10.5194/tc-5-349-2011>, 2011.
- Bookhagen, B. and Burbank, D. W.: Topography, relief, and TRMM-derived rainfall variations along the Himalaya, *Geophysical Research Letters*, 33, <https://doi.org/10.1029/2006GL026037>, 2006.
- Guillet, G., King, O., Lv, M., Ghuffar, S., Benn, D., Quincey, D., and Bolch, T.: A regionally resolved inventory of High Mountain Asia surge-type glaciers, derived from a multi-factor remote sensing approach, *The Cryosphere*, 16(2), 603-623, <https://doi.org/10.5194/tc-16-603-2022>, 2022.
- Haemmig, C., Huss, M., Keusen, H., Hess, J., Wegmüller, U., Ao, Z., and Kulubayi, W.: Hazard assessment of glacial lake outburst floods from Kyagar glacier, Karakoram mountains, China, *Ann. Glaciol.*, 55(66), 34-44, <https://doi.org/10.3189/2014AoG66A001>, 2014.
- Jiskoot, H.: Glacier Surging, in: *Encyclopedia of Snow, Ice and Glaciers*, edited by: Singh, V. P., Singh, P., and Haritashya, U. K., Springer Netherlands, Dordrecht, 415-428, [https://doi.org/10.1007/978-90-481-2642-2\\_559](https://doi.org/10.1007/978-90-481-2642-2_559), 2011.
- Markham, B. L., Storey, J. C., Williams, D. L., and Irons, J. R.: Landsat sensor performance: history and current status, *IEEE Trans. Geosci. Remote Sens.*, 42, 2691-2694, <https://doi.org/10.1109/TGRS.2004.840720>, 2004.
- Pitte, P., Berthier, E., Masiokas, M. H., Cabot, V., Ruiz, L., Ferri Hidalgo, L., Gargantini, H., and Zalazar, L.: Geometric evolution of the Horcones Inferior Glacier (Mount Aconcagua, Central Andes) during the 2002–2006 surge, *Journal of Geophysical Research: Earth Surface*, 121, 111-127, <https://doi.org/10.1002/2015JF003522>, 2016.
- Ragetli, S., Bolch, T., and Pellicciotti, F.: Heterogeneous glacier thinning patterns over the last 40 years in Langtang Himal, Nepal, *The Cryosphere*, 10(5), 2075-2097, <https://doi.org/10.5194/tc-10-2075-2016>, 2016.
- Round, V., Leinss, S., Huss, M., Haemmig, C., and Hajsek, I.: Surge dynamics and lake outbursts of Kyagar Glacier, Karakoram, *The Cryosphere*, 11(2), 723-739, <https://doi.org/10.5194/tc-11-723-2017>, 2017.
- Sevestre, H. and Benn, D. I.: Climatic and geometric controls on the global distribution of surge-type glaciers: implications for a unifying model of surging, *J. Glaciol.*, 61(228), 646-662, <https://doi.org/10.3189/2015JoG14J136>, 2015.
- Thayyen, R. J. and Gergan, J. T.: Role of glaciers in watershed hydrology: a preliminary study of a "Himalayan catchment", *The Cryosphere*, 4, 115-128, <https://doi.org/10.5194/tc-4-115-2010>, 2010.
- Truffer, M., Käab, A., Harrison, W. D., Osipova, G. B., Nosenko, G. A., Espizua, L., Gilbert, A., Fischer, L., Huggel, C., Craw Burns, P. A., and Lai, A. W.: Chapter 13 - Glacier surges, in: *Snow and Ice-Related Hazards, Risks, and Disasters (Second Edition)*, edited by: Haeberli, W., and Whiteman, C., Elsevier, 417-466, <https://doi.org/10.1016/B978-0-12-817129-5.00003-2>, 2021.

Zhang, Z., Zhao, J., Liu, S., Zhang, Q., Jiang, Z., Xu, Y., and Hu, K.: Characterization of Three Surges of the Kyagar Glacier, Karakoram, SSRN, <http://dx.doi.org/10.2139/ssrn.4065221>, 2022.

# Characterizing the surge behaviour and associated ice-dammed lake evolution of the Kyagar Glacier in the Karakoram

Guanyu Li<sup>1,2,3</sup>, Mingyang Lv<sup>1,2\*</sup>, Duncan J. Quincey<sup>4</sup>, Liam S. Taylor<sup>4</sup>, Xinwu Li<sup>1,2,3</sup>, Shiyong Yan<sup>5</sup>, Yidan Sun<sup>5</sup>, Huadong Guo<sup>1,2,3</sup>

5 <sup>1</sup>Key Laboratory of Digital Earth Science, Aerospace Information Research Institute, Chinese Academy of Sciences, Beijing 100094, China;

<sup>2</sup>International Research Center of Big Data for Sustainable Development Goals, Beijing 100094, China;

<sup>3</sup>University of Chinese Academy of Sciences, Beijing 100049, China;

<sup>4</sup>School of Geography, University of Leeds, Leeds, LS2 9JT, UK;

10 <sup>5</sup>Jiangsu Key Laboratory of Resources and Environmental Engineering, School of Environment Science and Spatial Informatics, China University of Mining and Technology, Xuzhou, 221116, China.

*Correspondence to:* Mingyang Lv (lmynju@163.com)

**Abstract.** Glacier surges are prevalent in the Karakoram and occasionally threaten local residents by inundating land and initiating mass movement events. The Kyagar Glacier is well-known for its surge history, and in particular its frequent-blocking  
15 of the downstream valley, leading to a series of high-magnitude glacial lake outburst floods. Although the surge dynamics of the Kyagar Glacier have been broadly described in the literature, there remains an extensive archive of remote sensing observations that have great potential for revealing specific surge characteristics and their relationship with historic lake outburst floods. In this study, we propose a new perspective on quantifying the surging process using successive Digital Elevation Models (DEMs), which could be applied to other sites where glacier surges are known to occur. Advanced  
20 Spaceborne Thermal Emission and Reflection Radiometer DEMs, High Mountain Asia 8-meter DEMs and the Shuttle Radar Topography Mission DEM were used to characterize surface elevation changes throughout the period [from](#) 2000 to 2021. We also used Landsat time-series imagery to quantify glacier surface velocities and associated lake changes over the course of two surge events between 1989 and 2021. Using these [data/datasets](#), we reconstruct the surging process of Kyagar Glacier in unprecedented detail and find a clear signal of surface uplift over the lower glacier tongue, along with uniformly increasing  
25 velocities, associated with the period of surge initiation. Seasonal variations in [surface](#) flow are still evident throughout the surge phase indicating the presence of water at the glacier bed. Surge activity [of Kyagar Glacier](#) is strongly related to the development and drainage of the terminal ice-dammed lake, which itself is controlled by the drainage system beneath the glacier terminus.

## 1 Introduction

30 A glacier surge is defined as a quasiperiodic oscillating glacial motion switching between rapid and slow flow, periods that are known as the active and quiescent phase respectively (Benn and Evans, 2010; [Jiskoot, 2011](#)). Surge-type glaciers account

for less than 1% of mountain glaciers, but they are important for studying ice flow instabilities and advancing knowledge of glacier processes and how they respond to a capricious climate (Benn, 2021; Clarke, 1987; Sevestre and Benn, 2015); [Truffer et al., 2021](#)). Surging glaciers are usually clustered, and are found within areas where inputs and outputs of enthalpy cannot keep balance (Benn et al., 2019). In this context, enthalpy refers to thermal energy and water gained at the glacier bed resulting from friction and geothermal heat. Sometimes, climate conditions, topographic and geologic features can intensify such imbalances. ~~The, and the~~ Karakoram is one such zone (Guillet et al., 2022; Sevestre and Benn, 2015). In contrast to most glacierised regions, the Karakoram has experienced balanced to slightly positive ice mass change in recent decades (Hewitt, 2005; Gardelle et al., 2013; Farinotti et al., 2020; Hugonnet et al., 2021), and surge activity has been common (Copland et al., 2011; Bhambri et al., 2017; Paul, 2020).

Glacier surges and related glacial lake outburst floods (GLOFs) occasionally cause catastrophic damage to local residents and infrastructure in high mountain regions of Asia (Hewitt and Liu, 2010; Bhambri et al., ~~2017~~[2019](#); Ding et al., 2018; Bazai et al., 2021). Most recently (2018-19) the Shispare Glacier in the central Karakoram surged, forming an ice-dammed lake (Rashid et al., 2020). The lake partially drained in June 2019 and then again in May 2020 affecting the Karakoram Highway and the neighboring village of Hasanabad (Bhambri et al., 2020). Similarly, the surge of Kelayayilake Glacier in the Pamir, which occurred in the spring of 2015, destroyed dozens of herders' huts and inundated valuable grazing meadow (Shangguan et al., 2016). A better understanding of surge dynamics, how they evolve, and their relationship with GLOFs would therefore be highly informative for local stakeholders.

Although among hundreds of other surge-type glaciers in the Karakoram, Kyagar Glacier has attracted a lot of attention in the literature (Haemmig et al., 2014; Round et al., 2017; Zhang et al., 2020). It is well known for blocking the Shaksgam valley and thus damming the river, which results in the formation of a large ice-dammed lake. It has been a threat over the past two centuries to more than one million people living in the Yarkant River basin (Yin et al., 2019). GLOFs caused by the Kyagar Glacier have been recorded by two gauging stations, at Kuluklangan and Kaqun, since the 1960s (Zhang, 1992; Haemmig et al., 2014). Attempts to provide an early warning system to alert local communities of an imminent flood have had limited success. Although the early warning station was submerged due to the rapid impoundment of the glacial lake in June, 2015, the system did warn the downstream communities and decision-makers about the coming GLOF (Haemmig et al., 2014; [Round et al., 2017](#)).

Previous work has focused on observational data and satellite images to characterize surface velocities and elevation changes over previous surge events ([Haemmig et al., 2014](#); Round et al., 2017; [Bhambri et al., 2019](#)) and to discuss their relationship with ice-dammed lake evolution. Round et al. (2017) drew the conclusion that outburst events at the Kyagar Glacier are controlled by basal and subglacial hydrological conditions. They also suggested that the potential for further GLOFs in the period following 2016 was high, ~~as the tongue continued to supply mass to the terminus area, maintaining the height of the existing ice dam~~. Haemmig et al. (2014) and Round et al. (2017) both inferred that previous surge activity had occurred prior to 2000, but did not give direct evidence of it. ~~Two former surges in the 1970s and 1990s were confirmed by Zhang et al. (2022) indicating an approximate surge cycle of 19-20 years~~ [They speculated that the recurring GLOFs recorded in 1978 and](#)

1999 could indicate the maximum return period of glacier surges. Bhambri et al. (2019) reported one of the surge events lasted from 1994 to 1997. Another former surge from 1975 to 1978 was confirmed by Zhang et al. (2022) using glacial velocity data derived from Landsat images, again indicating an approximate surge cycle of 19-20 years. Like other glacier surge studies utilizing remote sensing, most of them primarily focused on the evolution of surface velocity and description of related surface features, with limited DEMs used to discuss the amplitude of surface elevation change caused by the surges and analyse mass balance conditions.

Remote sensing images provide an excellent means of characterizing glacier ~~surface-conditions~~parameters, through the calculation of glacier flow fields and ~~mass-balance~~surface elevation changes for example. In particular, the long archive of Advanced Spaceborne Thermal Emission and Reflection Radiometer (ASTER) stereo images collected since 2000 can provide an insight into seasonal and annual changes in glacier surface elevation, especially for surge-type glaciers which experience more dramatic surface changes than non-surging glaciers. With a surge cycle comparable to the ASTER archive length, the Kyagar Glacier is an ideal case on which to test a new approach for describing glacier surge events using DEMs generated from ASTER images- (Pitte et al., 2016; Bhambri et al., 2019). The primary aim of this study was, therefore, to investigate the use of the ASTER archive to quantify glacier surge elevation change before, during, and after surge events. The High Mountain Asia 8-meter (HMA) DEMs (Shean, 2017a, 2017b) and the Shuttle Radar Topography Mission (SRTM) DEM (EROS Center, 2018) were added to narrow down uncertainties, with a view to developing a workflow that could be universal and popularized to other surging studies. As well as using an overall larger number of DEMs to reconstruct the surging process than previous studies (Pitte et al., 2016; Bhambri et al., 2019), we also applied HMA DEMs for the first time to better understand the evolution of the Kyagar Glacier surge.

To aid discussion of surge dynamics of Kyagar Glacier and GLOF assessment, we used Landsat time-series imagery to generate annual and monthly glacial surface velocity maps from 1989 to 2021 covering two surge events. In addition, we characterized the evolution of the ice-dammed lake up to 2022 and evaluated the potential for outburst floods emanating from this site in the future.

## 2 Study area

Kyagar Glacier is located on the southern slope of Shaksgam Valley near the boundary of Tarim River basin and Indus River basin (Fig. 1). To the northwest of Kyagar Glacier stands Mount Chogori, known as 'K2'. The glacier is polythermal in nature (Shi and Liu, 2000) and the meltwater that is discharged from the Kyagar Glacier supplies the Keleqin River, which is the largest tributary of Yarkant River. Regional temperatures range from -25 °C to +10 °C and the peak melt season runs from June to September (Zhang et al., 2020). Records from meteorological stations in the neighboring Tibet Plateau and Tarim Basin show an increase of ~2 °C in mean annual temperature since the 1960s (Lv et al., 2020a). Precipitation in this region is primarily controlled by the Asian monsoon during summer months, and westerly circulation during winter months (Beleh et al., 2012).Bookhagen and Burbank, 2006; Thayyen and Gergan, 2010). Due to its continental nature and high

elevation situation, there is relatively little precipitation to nourish the glacier accumulation zone. Precipitation of just 8.87 mm a<sup>-1</sup> was recently recorded by the Kyagar automatic monitoring station at an elevation of 4810 m above sea level (a.s.l.) (Wei et al., 2018) (Fig. 2c).

Composed of three tributaries, Kyagar Glacier has a glacierized area of 97.3 km<sup>2</sup>, flowing from its maximum elevation of 7196 m a.s.l. down to the glacier terminus at 4738 m a.s.l. It is at the glacier terminus where small fluctuations in ice flux can result in a blockage of the Keleqin River in the Shaksgam Valley, and the formation of an ice-dammed lake (Fig.2a). Meltwater from several other glaciers in the broader catchment also contribute to the lake volume. Glacier centerline elevation profiles (Fig. 2a) show that the western branch is higher than the central branch above the confluence (Fig. 2b). The glacier hypsometry indicates a bottom-heavy morphology (Fig. 2c). The glacier tongue is densely covered by ice crevasses and ice pinnacles, but there is a general absence of ‘classic’ surge-type surface features (e.g. looped-moraines) (Copland et al., 2003; Sevestre and Benn, 2015).

## 110 3 Data and methods

### 3.1 Multi-source remote sensing data

We used three DEM products in addition to Landsat series satellite imagery to facilitate this study (Table 1). DEMs were mostly derived from stereo ASTER imagery and supplemented by the HMA DEM and the SRTM DEM. In total we compiled 85 DEMs presenting elevation conditions from 2000 to 2021. These DEMs were co-registered and differenced to generate elevation change maps over the glacierized area and surrounding stable terrain. Post-processing was conducted to identify the glacier surge period and quantify elevation changes before, during, and after the surge on a pixel level. 373 images acquired by Landsat 5 TM, Landsat 7 ETM+, and Landsat 8 OLI were collected to extract annual and monthly glacial surface velocities and investigate glacial lake evolution between 1989 and 2021.

#### 3.1.1 ASTER DEM

The Terra ASTER DEM, also known as the AST14DEM data product (NASA/METI/AIST/Japan Spacesystems and U.S./Japan ASTER Science Team, 2001), is produced by the Land Processes Distributed Active Archive Center (LP DAAC) using two stereo images in the near-infrared (Bands 3N and 3B). AST14DEM images have a spatial resolution of 30 m under the Universal Transverse Mercator (UTM) coordinate system and is more accurate than 25 m root mean square error in all dimensions. The ASTER DEM product was ordered through NASA’s Earthdata Search (<https://search.earthdata.nasa.gov>). In this study, the acquisition dates of 67 ASTER DEMs with less than 75% cloud cover are evenly spread between February 2001 and September 2021 (Table S1). Having a width of 60 km, a single granule was sufficient to cover the entire Kyagar Glacier. Therefore, we used the ASTER DEM as the primary data source for quantifying surface elevation changes.

### 3.1.2 HMA DEM

130 The HMA DEM dataset is generated from stereoscopic DigitalGlobe satellite imagery released by the National Snow and Ice  
Data Center (NSIDC) in 2017 (Shean, 2017a, 2017b). Benefiting from the high spatial resolution of predominantly commercial  
satellites, the HMA DEM has a finer resolution of 8 m than the ASTER DEM. Seventeen HMA DEM strips (with cloud cover  
lower than 75%) cover the Kyagar Glacier with a temporal coverage from June 2011 to October 2016 (Table S1). Before co-  
135 registration, these DEMs were resampled to 30 m and reprojected to the UTM grid as per the ASTER ~~and SRTM DEM~~ DEMs.  
Due to the fewer number than ASTER DEMs, HMA DEMs were taken as the supplementary data for quantifying surface  
elevation changes (Table S1).

### 3.1.3 SRTM DEM

140 The Shuttle Radar Topography Mission (SRTM) collected near-global C-band radar data during 11 days in February 2000.  
Two different radar antennas onboard the shuttle formed a single-pass interferometry, which was used to calculate surface  
elevation. ~~Released by United States Geological Survey (USGS) in 2015, SRTM 1 are second global DEM (version 3.0)~~ The  
SRTM DEM has an accuracy better than 10 m in both horizontal and vertical directions, at least in areas of low relief (Farr et  
al., 2007). ~~The SRTM DEM~~ We used SRTM Non-Void Filled DEM released by United States Geological Survey (USGS) in  
which the data gaps are neither interpolated nor filled using other DEMs. The SRTM DEM was resampled to 30 m and  
reprojected to the UTM grid. It was used as reference elevation for co-registration with other DEM datasets. Penetration of the  
145 radar signal can be up to several meters in snow- and ice-covered areas leading to uncertainty in the surface elevation retrieval  
(Rignot et al., 2001), ~~but the impact of this is small when compared to the elevation changes caused by a surge event~~ 2001). In  
order to correct for surface penetration, we applied adjustments of +5.5 m over firn and snow areas and +1.1 m over clean ice  
areas following previous studies in the nearby region (e.g. Lv et al., 2020a). Identification of ice and snow facies is based on  
a Landsat ETM+ image acquired in February 2000, which was approximately coincident with the SRTM mission.

### 3.1.4 Landsat series imagery

150 As the longest continuous satellite mission observing the Earth, Landsat imagery is perfect for monitoring environment  
evolution over the past half century. As a consequence of coarse spatial resolution and data scarcity, images acquired by  
Landsat-1, -2, and -3 with resolution of approximate 60 m would be extremely challenging for feature tracking. Therefore, a  
total of 373 radiometrically and geometrically corrected images from Landsat 5, 7 and 8 imageries were downloaded from  
USGS Earth Resources Observation and Science Center (EROS) (<https://glovis.usgs.gov/>) (Wulder et al., 2022) to investigate  
155 glacial lake area changes. Additionally, feature tracking was applied to all acquired images and the results from 60 pairs with  
good correlation performance were finally selected to present annual surface displacements from 1989 to 2021 as well as  
monthly displacements during surge events.

### 3.2 DEM co-registration and outlier filtering

160 Multi-source DEMs are known to have inconsistent geolocations due to varying data acquisition models, inadequate ground  
survey conditions, different data post-processing methods, and other sources (Nuth and Kääb, 2011). Following the workflow  
in Figure 3, we co-registered the ASTER DEMs and HMA DEMs to the reference SRTM DEM using Nuth and Kääb (2011)  
and demcoreg (Shean et al., 2016). Demcoreg is a collection of Python and shell scripts for co-registration of DEMs, which  
automatically implements the correction algorithm [by Nuth and Kääb \(2011\)-using areas of stable terrain, where the DEMs  
are least error-prone \(Berthier et al., 2016\)](#). The mean and standard deviations of DEM offsets over off-glacier areas before  
165 and after co-registration are shown in Table S1. After the co-registration, we resampled all DEMs to the resolution of the  
~~coarsest~~ ASTER DEM (30 m) using a cubic convolution interpolation, and then we generated difference maps between  
ASTER/HMA DEMs and the reference SRTM DEM in order to obtain regional elevation change data.

To remove outliers in each elevation-change map, glacierised and non-glacierised areas were handled separately. Non-glacier  
pixels with values greater than 3 standard deviations from the mean were discarded (Ragetti et al., 2016), and the vertical  
170 offsets of most selected ASTER/ HMA DEMs relative to SRTM over [stable non-glacierised](#) terrain were reduced to within  $\pm$   
2 m. We assumed elevation changes over the accumulation zone did not exceed 3 m in each year from 2000 to 2021 and  
therefore filtered pixels above 5600 m a.s.l. with values  ~~$\pm 63$~~  [accounting for each timestep \(e.g., for a 10 year interval, the filter  
value was  \$\pm 30\$  m\)](#) (Lv et al., ~~2020~~2020b). Pixels at elevations below 5600 m a.s.l. were filtered with a threshold of  $\pm 150$  m to  
avoid excluding real values associated with surging. Outlier-free elevation change maps were arranged in chronological order  
175 ready for further processing.

### 3.3 Post-processing of DEM differencing data

Using the elevation change data of Kyagar Glacier as a basis, we here present a time series processing method for long-term  
elevation change monitoring and for the detection of possible surge events.

180 The Bayesian Estimator of Abrupt change, Seasonality and Trend (BEAST) is a Bayesian model averaging algorithm to  
decompose time series data into components, including seasonality, trend, and abrupt changes (Zhao et al., 2019). Compared  
with conventional change point detection algorithms, BEAST does not seek a single best model that may result in poor fitting,  
but rather combines kinds of models into an ensemble model and fits the seasonal and trend signals based on Bayesian model  
averaging and Markov Chain Monte Carlo strategies (Cai et al., 2020). Applying the BEAST model to DEM differencing data  
over Kyagar Glacier pixel by pixel, we fitted trend signals and located periods of abnormal change from 2000 to 2021, on a  
185 six-month rolling basis (Fig. 4). Given that BEAST is a general linear regression model using Bayesian probability, we  
evaluated its performance by common measures such as probability, R-square ( $R^2$ ), and root-mean-square error (RMSE). [The  
abnormal changes in an time-series elevation data were identified by the probability parameters, which are calculated by  
summing the probability distribution in the trend signals \(Fig. 4b,e,h,k\). According to IPCC Likelihood Scale, the abnormal  
elevation change is 'more likely than not' to occur when the probability is greater than 0.50 \(Mastrandrea et al., 2010\).](#)

190 [Therefore, we suggest the pixels with probability value larger than 0.50 are credible enough to be considered as abnormal changes.](#) We also compared the findings from BEAST to the known timing of surge events as recorded in the literature.

We then applied the PieceWise Linear Functions (PWLf) Python package to further decompose the trend in elevation change into multiple piecewise linear function models (Jekel and Venter, 2019). PWLF is based on a differential evolution optimization algorithm, where users can specify the location or numbers of break points (Storn and Price, 1997). For linear  
195 function models, the slope of each segment represents the elevation-change rate within the corresponding period, and the breakpoints represent the abrupt ~~time of elevation~~-change [time](#) resulting from the glacier surge event.

The results of the BEAST process clearly indicated the presence of a surge event between 2010 and 2018. Thus, we limited the detection of break points to this period. After the PWLF process, every pixel over Kyagar Glacier was assigned 6 parameters; elevation-change rates before, during, and after the surge, the dates of surge initiation and termination, and the  
200 duration of the surge impact using labels of  $k_1$ ,  $k_2$ ,  $k_3$ ,  $T_s$ ,  $T_e$ , and  $I$  respectively (Fig. 3, Fig. 4i).

### 3.4 Extraction of glacial velocities

In order to measure surface displacements, feature tracking was conducted using COSI-Corr (Leprince et al., 2007). After co-registration, image pairs were cross-correlated using a sliding window between  $32 \times 32$  and  $8 \times 8$  to measure horizontal displacements between corresponding surface features along the north-south and east-west directions. Glacial velocity ( $Vel$ )  
205 was then calculated through Eq. (1).

$$Vel = \frac{D_y \times \sqrt{P_{n-s}^2 + P_{e-w}^2}}{D_i} \quad (1)$$

Where:

$D_i$  is the period in days between acquisition of each image pair and  $D_y$  is assigned 365 which is the number of days in a year.  $P_{n-s}$  and  $P_{e-w}$  are the displacements in north-south and east-west directions respectively. Panchromatic bands of Landsat-7  
210 and Landsat-8 with a resolution of 15 m were selected as the potential image pairs between 1999 and 2021. [Despite the Scan Line Corrector failure in May 2003 \(Markham et al., 2004\), we found that feature tracking of Landsat-7 image pairs from 2003 to 2013 was still viable for tracking features between the data gaps.](#) To cover the period before 1999, band 4 of Landsat-5 was used as features over ice and snow are more recognizable in the near-infrared spectrum. Velocity profiles along centerlines of west and central branches in Figure 2 were extracted and presented in chronological order so as to consider variabilities among  
215 different years and during surge events. We manually removed blunders with differences more than  $20 \text{ m a}^{-1}$  compared to surrounding areas in each velocity profile. It has previously been shown this method is applicable for velocity analysis of mountain glaciers with varying degrees of debris cover (Lv et al., 2019).

~~Despite the Scan Line Corrector failure in May 2003 (Markham et al., 2004), we found that feature tracking of Landsat-7 image pairs from 2003 to 2013 was still viable for tracking features between the data gaps.~~

### 220 3.5 Uncertainty of velocity extraction

We took the residual velocity value over ice-free regions as the uncertainty of the velocity extraction. Landsat sensors have different spectral features and spatial resolutions leading to different correlation qualities between image pairs. We generated detailed residual value statistics on hillside and valley areas for the three image categories. The mean uncertainties of Landsat 7 and Landsat 8 image correlation results were 1.29 m a<sup>-1</sup> and 0.69 m a<sup>-1</sup> respectively, with standard deviations of 5.36 m a<sup>-1</sup> and 1.01 m a<sup>-1</sup>. Correlation results of Landsat 5 were a little worse having a mean uncertainty of 6.72 m a<sup>-1</sup> and a standard deviation of 7.12 m a<sup>-1</sup>. Considering that the annual velocities of Kyagar Glacier reach more than 50 m a<sup>-1</sup> even during the quiescent phase, we consider those uncertainties acceptable for studying Kyagar Glacier motion characteristics.

### 3.6 Visual interpretation of ice-dammed lake evolution

230 We investigated the area of the ice-dammed lake using visual interpretation of satellite images. 148 Landsat images were selected and manually digitised to extract near-monthly lake boundaries (Fig. S1-S11). The HMA DEM obtained on 13 January 2013, when the lake was completely discharged, was taken as reference DEM. We assumed the lake bed remained stable during the studied period, and the lake surface elevations at different times were then estimated using the extracted lake boundaries and the reference HMA DEM.

## 4 Results

### 235 4.1 Surging characteristics

Velocity data indicate that the western branch of Kyagar Glacier experienced two surges from 1989 to 2021, and this was validated by visual interpretation. ~~One~~The first surge occurred from 1992 to 1998 and the ~~other~~second surge from 2012 to 2019, confirming the previously inferred return period of ~20 years (Fig. 5.6). The first surge peaked in November 1995 following three years of acceleration and declined thereafter to a minimum level over the next three years. The second surge peaked in September 2014 after a two-year acceleration and declined to a minimum over the next five years (Fig. 6.7,8).

240 The two surges both reached a peak monthly velocity of ~800 m a<sup>-1</sup>, 2-6 km from the terminus (Fig. 6a7a,c). During the quiescent phase (i.e. before 1992 and from 2000 to 2012), the western branch had an average annual velocity of 40-80 m a<sup>-1</sup> (Fig. 5c,d). Velocities of the two branches differed above the confluence (after 7 km) and the central part of the tongue also experienced coincident acceleration and deceleration, albeit at a slightly slower rate (Fig. 5a,b,e,f). This implies the surging activity of the western branch did not block the motion of the central branch, rather it promoted ice mass transportation of the central branch to some extent.

245 Monthly velocity profiles provide more detail of the dynamic evolution of the surge during the active phase. Figure 6a7d suggests that seasonal variations in flow are still an important control on velocity rates, peaking during April to October. The two surges both exhibit abrupt acceleration after spring (2014/04-2014/06 in Fig. 6a7a and 1995/04-1995/11 in Fig. 6e7c, Fig.

250 8). They reached a maximum by the end of the same year and started to decline at the beginning of the next year (2014/10-2015/01 in Fig. 6b7b and 1996/02-1996/04 in Fig. 6e7c, Fig. 8). However, the deceleration was temporally variable; abnormal increases in both 2015/06-2015/07 and 1996/05-1996/09 suggest this was not a single event of summer re-acceleration after the peak velocity in winter: (Fig. 8).

Kyagar Glacier entered the quiescent phase after 1998. The large volume of ice in the receiving zone rapidly ablated and the reservoir began to recharge, preparing for the next surge (Fig. 7a9a). During the period 2012 to 2016, the second surge event occurred. The surface elevation of the central branch lowered by 20-30 m in the accumulation zone, evidencing that the surge impact was wider than just on the western branch (Fig. 7b9b). This is consistent with the velocity profiles, which show that the central branch also experienced surge-like acceleration and deceleration. Although the active phase ended in 2020, part of the reservoir zone had already started to recharge during the latter part of the surge (Fig. 7e9c).

260 The multi-temporal DEM analysis (Section 3.3) revealed that elevation-change rates in the quiescent phase ( $k_1$ ) reached 53 to 75 m a<sup>-1</sup> in the reservoir and -7 to -9 m a<sup>-1</sup> in the receiving zone (Fig. 8a10a). During the surge, change rates ( $k_2$ ) had peak values ranging from -45 to -55 m a<sup>-1</sup> in the reservoir and 55 to 65 m a<sup>-1</sup> in the receiving zone (Fig. 8b10b). In the following few years after the surge impact, change rates ( $k_3$ ) were 43 to 76 m a<sup>-1</sup> in the reservoir and -31 to -52 m a<sup>-1</sup> in the receiving zone (Fig. 8e10c). Elevation-change rates right after the surge event (Fig. 8e10c) are lower than those during the entire quiescent phase (Fig. 8a10a). It is notable that only the lower region (0-4 km from the terminus) and another area (7-10 km from the terminus) exhibited abnormal elevation changes, while changes over the glacier surface 4-7 km from the terminus were small during the surge. [This unclear change signal could result from the limited quality of the DEMs at this time.](#)

Results of  $k_1$ ,  $k_2$ , and  $k_3$  suggest many pixels over Kyagar Glacier did not experience abrupt elevation changes. Therefore, we only show here the surge initiation ( $T_s$ ) and termination ( $T_e$ ) of the pixels with probabilities greater than 0.5 in the BEAST process. The earliest  $T_s$  was in 2012 detected over part of the receiving zone (Fig. 8d10d). The latest  $T_e$  was in 2017 at the edge of the terminus (Fig. 8e10e).

#### 4.2 Evolution of the ice-dammed lake

~~We investigated the evolution of the ice-dammed lake using visual interpretation of satellite images and the SRTM DEM (Fig. S1-S11).~~ The lake exhibited an irregular change from 1989 to 2021 (Fig. 911). In the early 1990s, the lake remained stable and grew slowly. From 1996 to 2009, the lake experienced yearly oscillations both in area and surface elevation. Before 2000, the annual maximum area of the lake exceeded 2 km<sup>2</sup> and reached the maximum of 3.21 km<sup>2</sup> in September 1998. ~~Within two days of~~ After reaching ~~the~~ its maximum area ~~in each year~~, the lake discharged almost entirely ~~within about two days~~, likely resulting in annual GLOFs to the downstream valley- ~~from 1996 to 2009~~. No lake existed between 2009 and 2015 suggesting an open channel developed beneath the glacier. From 2015 to 2021, the lake entered another period of yearly oscillations reaching a maximum area of 2.76 km<sup>2</sup> in August 2017. In contrast to the earlier period, the lake did not fully disappear, ~~and the during each drainage event. The~~ timing of each reduction in lake area suggests historic lake outbursts ~~usually~~ took place during every summer ~~since 1996~~ (July to September).

## 5 Discussion

### 5.1 Surging process of Kyagar Glacier

285 The semi-automated parameters extracted from successive DEMs have the advantage of being objectively derived and appear to show a clearer pattern than the elevation change descriptions that former studies have relied on. Combining these values with the velocity profiles, we could robustly rebuild the surging process during the last decade.

At the beginning of the surge, velocities increased uniformly and slowly along the glacier tongue, ~~with no~~ [since October 2012](#) (Fig. [5e, 6](#)). ~~It was not until April 2014 that an~~ obvious surge front ~~forming until April 2014~~ [formed](#) (Fig. [5e, 6a, 7a, 8](#)), a pattern  
290 which was also recorded by Round et al. (2017). However, the surge front did not impact the terminus, most likely due to frictional stress at the bed and the disconnected englacial hydrological system (Björnsson, 1998). ~~There was a zone of intense compression.  $T_s$  values in 2012 and 2013 were detected over the area~~ 3-4 km from the terminus ~~resulting in~~ (Fig. 10d), indicating a notable elevation increase. ~~Consequently,  $T_s$  values in 2012 and 2013 were detected over the~~, which we speculate resulted [from intense compression of ice that could not be transported into the](#) middle part of the receiving zone ~~(Fig. 8d)~~, while  
295 elevations over the reservoir zone had no obvious change during this period (Fig. [4012](#)).

The surge front was clearly evident in the velocity profiles after April 2014 (Fig. [6a, 7a](#)). The previous surge in the 1990s also underwent abrupt acceleration after spring (April 1995) (Fig. [6e, 7c, 8](#)). We suggest this [spring speed-up](#) could be attributed to two reasons. The first relates to a reduction in till strength brought about by an increase in water at the bed during spring, as discussed in previous studies (Cuffey and Paterson, 2010; Round et al., 2017). The second relates to the extrusion stress of the  
300 accumulated ice in the receiving zone during 2012 and 2013, which likely reached the deformation threshold. The abrupt speed-up along the entire glacier tongue caused the reservoir surface started to rapidly decline in 2014, transporting a massive volume of ice to the receiving zone (Fig. [4012](#)).

Velocities reached a maximum of  $\sim 800 \text{ m a}^{-1}$  in October 2014 and declined again in the coming winter and spring (Fig. [6b, 7b, 8](#)). However, velocities increased again in June-August of 2015, which is coincident with the summer speed-up that is evident  
305 in the quiescent phase. Re-acceleration after the peak velocity was also found in May-September of 1996 during the previous surge (Fig. [6e, 7c, 8](#)). We suggest seasonal variations could still play a role in controlling glacial motion during surges. After the summer of 2015, velocities decreased rapidly to  $\sim 200 \text{ m a}^{-1}$  within one year and decreased slowly henceforth from 2016 to 2019 (Fig. 5f). In the meantime, a mass wave was generated in the receiving zone propagating towards the terminus (Fig. [8d, 10d, e](#)).

310 We interpret the surge initiation most likely coincided with the maximum volume of ice that could be stored in the reservoir zone being exceeded, as suggested by Barrand and Murray (2006). The reservoir zone was at capacity at the end of quiescent phase and transported more ice to downstream than before causing a slow and uniform speed-up from the reservoir to the receiving zone. Hydrologic processes within and beneath the glacier became important at the same time the surge front was formed. Once the surge front had passed through the system and the reservoir zone was largely drained, the glacier resumed  
315 its quiescent state, still maintaining a basal hydrology, but with much reduced effect.

## 5.2 Methodological consideration of DEM difference post-processing

The identification of the surge period (2012-2017) using multi-temporal DEM processing is shorter than that when using velocity profiles alone (2012-2019). This can most likely be attributed to the nature of the method. Specifically, we identified the lattermost profile (2019/08-2020/09 in Fig. 5f) with a decreasing velocity as the surge termination, even though the reduction may have been small (e.g.  $<10 \text{ m a}^{-1}$ ). The consequent effect of such velocity changes on the surface elevation would go undetected given the vertical resolution of our data, meaning this period was likely already defined as the start of quiescent phase in PWLF process. The duration of the surge impact ( $I$ ) on individual pixels varied from one to three years (Fig. 10f), meaning that the surge affected most parts of the glacier for discrete periods, rather than for the whole of the active phase.

Uncertainties of elevation change point detection and elevation change rate calculation raised from the processing of BEAST model and PWLF model are shown in Figure 13. For the BEAST model, there exists three parameters to evaluate the uncertainties of the model processing, including the occurrence probability of abnormal change over time, regression evaluation parameters such as  $R^2$  and RMSE, as well as the estimated variance of the model error (Zhao et al., 2019). For the PWLF model, various statistics can be calculated if we assume that the breakpoint locations and model form are correct. Similar to the BEAST model, the PWLF model provides the  $R^2$  and standard deviation based on prediction variance to evaluate the uncertainty due to the lack of data in the time series (Jekel and Venter, 2019).

In both models, the output result will be nan/null if the model fitting fails or identified change points are not enough. Possible failure reasons include poor data quality, too few data points in time series, or too little variation in the time series. A lower number of null values and highly concentrated valid pixel distributions over the glacier region, indicate a higher reliability of the model analysis results. As shown in Figure 13, valid pixels are filled in the flatter, lower part of the glacier, while many null pixels exist at high elevation and over steep slopes. This means the model has higher reliability over glacier tongue.

The BEAST and PWLF models are based on general linear regression, so we evaluated the performance of the time series fitting and change point detection by regression parameters including  $R^2$  and standard deviation. There are a large number of pixels with high standard deviation and low  $R^2$  in the higher part of glacier (Fig. 11a,b,d,e). Due to the BEAST and PWLF model processing order, 13a,b,d,e).  $R^2$  in PWLF is higher than that in BEAST, while the standard deviation in PWLF is less than that in BEAST. On the other hand, as the processing BEAST model is firstly conducted to process the time-series DEMs, the results of BEAST model could contain more information about the raw data quality and spatial-temporal distribution in time series. However, the coefficient of determination does not necessarily reflect the accuracy of detecting true trend change points (TCPs) in time series. HereAs introduced in Section 3.3, the BEAST algorithm evaluated not only the most likely timings and numbers of TCPs at any given time for each pixel in the glacier, but also the probability of each TCP being true (Zhao et al., 2019). Compared to the linear regression processing, the detection of TCPs is much stricter. As a result, the pixels with higher  $R^2$  and lower standard deviation does not necessarily mean high probability of the TCP being true. In Kyagar Glacier, the pixels with high abnormal change probability ( $\geq 0.5$ ) were mainly detected in the reservoir and receiving regions.

Although the uncertainty of this approach requires further evaluation, it can quantify surging process in an unprecedented detail. Using this approach, we can investigate elevation-change rates during each period of surge-type glacier, the time of surge initiation and termination, and the surge duration. Compared to manually identifying surges from abrupt changes in DEMs, this approach is much more efficient and objective, only consuming a certain amount of computation load. It would be a valuable attempt to extend the approach to other surge-type glaciers of the whole HMA and even globally, which also makes it possible to identify surge events in a semi-automatic manner based on elevation change data. [The only limiting factor for applying this approach would be that a large amount of DEMs with good spatial and temporal coverage are needed.](#)

### 355 **5.3 Relationship between ice-dammed lake and surges**

Previous studies revealed the ice-dammed lake outbursts were related with dynamics of Kyagar Glacier, especially surging events (Haemmig et al., 2014; Zhang et al., 2020). By providing detailed lake evolution data we can offer more comprehensive insights into the relationship between surge and lake outburst events.

We identified two oscillating periods of lake area and surface elevation, which occurred from 1996 to 2009 and 2015 to 2021. Round et al. (2017) also suggested historic lake outbursts could indicate surge activities of Kyagar Glacier. The lake burst every year during these two periods, although not every GLOF was detected at the gauging station hundreds of kilometers downstream (Chen et al., 2010). This suggests the surge was not the direct reason for triggering the GLOFs. However, we did find a relationship between them, which is that the ice-dammed lakes reached maximum areas after three years when the surge peaked in velocities. For instance, the velocity peaked in 1995 with a maximum lake area of 3.21 km<sup>2</sup> in 1998, and in the next surge, velocity peaked in 2014 with a maximum lake area of 2.76 km<sup>2</sup> in 2017. We suggest that it would take three years for the terminus to build a sufficiently large barrier for the lake to develop to its greatest extent after the surge peak.

As a polythermal glacier, it is likely that the nature and efficiency of the hydrological system of the glacier varies greatly on a seasonal basis. Lakes from 1996 to 2009 nearly disappeared every time after outbursts. We suggest that the lake forged an englacial channel through the dam every summer. This interpretation is supported by an evident residual channel in the downstream valley flowing from the terminus area without any obvious changes on the glacier surface (Fig. S1-S6).

Most lake areas from 2015 to 2021 were smaller than during the previous cycle, suggesting the danger associated with the outburst events could be diminishing. During this period, the lake drainage events did not entirely empty the basin (Fig. 911, Fig. S7-S11). This was probably because the connected channel was part way up the ice dam such that the lower part of the lake could not drain. It is therefore likely that it was the alteration of the drainage system beneath (or within) the glacial terminus that controlled the occurrence of each individual GLOF event.

## **6 Conclusion**

Using SRTM, ASTER and HMA DEMs, as well as Landsat time-series images, we detected and described the vertical and horizontal glacial motion of Kyagar Glacier and assessed its relationship with GLOFs. By proposing a new quantifying

approach based on patterns shown in successive DEMs and combining velocity profiles during last three decades, we  
380 constructed the surging process of Kyagar Glacier in an unprecedented detail. As the first aim of this study, (1) we suggest the  
new quantifying approach of surging activities basing on the BEAST and PWLF processes could be popularized to other surge-  
type glaciers in the HMA or specific regions of Arctic ring. We also find that (2) abnormal uplift over the lower glacier tongue,  
combined with a uniform increase in velocities, is the clearest indicator of surge initiation. (3) Seasonal variations in flow  
could still play a role in controlling glacial motion during surges. (4) Surge activities have a strong relationship with the ice-  
385 dammed lake evolution, but it is likely to be the alteration of the drainage system within the terminus area that triggered the  
GLOF events.

*Data availability.* The Landsat series images are available from <https://glovis.usgs.gov/> (last access: 10-28-2022). ASTER DEMs can be  
freely downloaded from <https://search.earthdata.nasa.gov> (last access: 10-28-2022). ~~SRTM DEM is from USGS EROS Archive. HMA  
390 DEMs are provided by NASA NSIDC.~~ SRTM DEM is from USGS EROS Archive ([https://www.usgs.gov/centers/eros/science/usgs-eros-  
archive-digital-elevation-shuttle-radar-topography-mission-srtm-non](https://www.usgs.gov/centers/eros/science/usgs-eros-<br/>archive-digital-elevation-shuttle-radar-topography-mission-srtm-non), last access: 03-19-2023). HMA DEMs are provided by NASA NSIDC  
([https://nsidc.org/data/hma\\_dem8m\\_mos/versions/1](https://nsidc.org/data/hma_dem8m_mos/versions/1), last access: 03-19-2023).

*Supplement.* The supplementary document related to this article is available online at:.

*Author contributions.* ML, DJQ, XL, and HG designed this study. GL, LST, and ML carried out the data processing. ML, GL, and DJQ  
wrote the manuscript. SY and YS edited every version of this manuscript and assisted in data analyzing.

395 *Competing interests.* The authors declare that they have no conflict of interest.

*Acknowledgements.* This research is supported by ~~the Strategic Priority Research Program of the Chinese Academy of Sciences  
(XDA19070202), the National Natural Science Foundation of China (42101124),~~ the Innovative Research Program of the International  
Research Center of Big Data for Sustainable Development Goals (CBAS2022IRP03, [CBAS2022IRP02](#)), ~~the National Natural Science  
400 Foundation of China (42101124), the Strategic Priority Research Program of the Chinese Academy of Sciences (XDA19070202),~~ and the  
International Partnership Program of the Chinese Academy of Sciences (183611KY5B20200059). We greatly thank related organizations  
and departments for providing data used in this study. We acknowledge the help of Drs. Fanny Brun and Evan Miles for their support on a  
previous version of this manuscript.

## References

Barrand, N. E. and Murray, T.: Multivariate Controls on the Incidence of Glacier Surging in the Karakoram Himalaya, *Arct.*  
405 *Antarct. Alp. Res.*, 38(4), 489-498, [https://doi.org/10.1657/1523-0430\(2006\)38\[489:MCOTIO\]2.0.CO;2](https://doi.org/10.1657/1523-0430(2006)38[489:MCOTIO]2.0.CO;2), 2006.

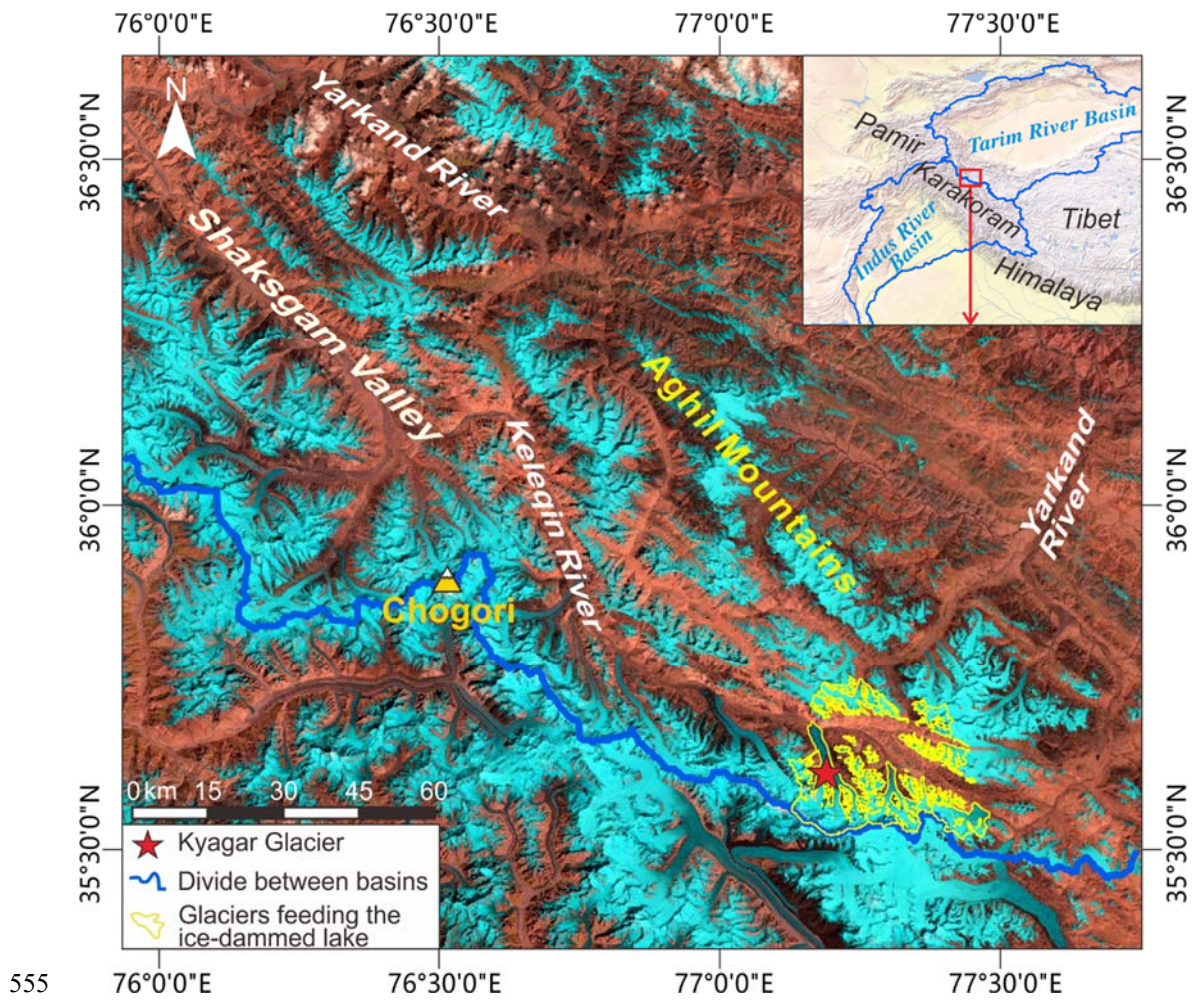
- Bazai, N. A., Cui, P., Carling, P. A., Wang, H., Hassan, J., Liu, D., Zhang, G., and Jin, W.: Increasing glacial lake outburst flood hazard in response to surge glaciers in the Karakoram, *Earth-Sci. Rev.*, 212, 103432, <https://doi.org/10.1016/j.earscirev.2020.103432>, 2021.
- 410 Benn, D. I.: Surging glaciers in Scotland, *Scott. Geogr. J.*, 137(1-4), 1-40, <https://doi.org/10.1080/14702541.2021.1922738>, 2021.
- Benn, D. I. and Evans, D. J. A. (Eds.): *Glaciers and glaciation*, London: Hodder Education, 2010.
- Benn, D. I., Fowler, A. C., Hewitt, I., and Sevestre, H.: A general theory of glacier surges, *J. Glaciol.*, 65(253), 701-716, <https://doi.org/10.1017/jog.2019.62>, 2019.
- 415 [Berthier, E., Cabot, V., Vincent, C., and Six, D.: Decadal Region-Wide and Glacier-Wide Mass Balances Derived from Multi-Temporal ASTER Satellite Digital Elevation Models. Validation over the Mont-Blanc Area, \*Front. Earth Sci.\*, 4, <https://doi.org/10.3389/feart.2016.00063>, 2016.](https://doi.org/10.3389/feart.2016.00063)
- Bhambri, R., Hewitt, K., Kawishwar, P., and Pratap, B.: Surge-type and surge-modified glaciers in the Karakoram, *Sci. Rep.*, 7(1), 15391, <https://doi.org/10.1038/s41598-017-15473-8>, 2017.
- 420 [Bhambri, R., Hewitt, K., Kawishwar, P., Kumar, A., Verma, A., Snehmani, Tiwari, S., and Misra, A.: Ice-dams, outburst floods, and movement heterogeneity of glaciers, Karakoram, \*Global Planet. Change\*, 180, 100-116, <https://doi.org/10.1016/j.gloplacha.2019.05.004>, 2019.](https://doi.org/10.1016/j.gloplacha.2019.05.004)
- [Bhambri, R., Watson, C. S., Hewitt, K., Haritashya, U. K., Kargel, J. S., Pratap Shahi, A., Chand, P., Kumar, A., Verma, A., and Govil, H.: The hazardous 2017–2019 surge and river damming by Shispare Glacier, Karakoram, \*Sci. Rep.\*, 10\(1\), 4685, <https://doi.org/10.1038/s41598-020-61277-8>, 2020.](https://doi.org/10.1038/s41598-020-61277-8)
- 425 Björnsson, H.: Hydrological characteristics of the drainage system beneath a surging glacier, *Nature*, 395(6704), 771-774, <https://doi.org/10.1038/27384>, 1998.
- [Boleh, T., Kulkarni, A., Kääh, A., Huggel, C., Paul, Bookhagen, B. and Burbank, D. W.: Topography, relief, and TRMM-derived rainfall variations along the Himalaya, \*Geophys. Res. Lett.\*, 33, <https://doi.org/10.1029/2006GL026037>, 2006.](https://doi.org/10.1029/2006GL026037)
- 430 ~~[F., Cogley, J. G., Frey, H., Kargel, J. S., Fujita, K., Scheel, M., Bajracharya, S., and Stoffel, M.: The State and Fate of Himalayan Glaciers, \*Science\*, 336\(6079\), 310-314, <https://doi.org/10.1126/science.1215828>, 2012.](https://doi.org/10.1126/science.1215828)~~
- [Boleh, T., Pieczonka, T., and Benn, D. I.: Multi decadal mass loss of glaciers in the Everest area \(Nepal Himalaya\) derived from stereo imagery, \*The Cryosphere\*, 5\(2\), 349-358, <https://doi.org/10.5194/te-5-349-2011>, 2011.](https://doi.org/10.5194/te-5-349-2011)
- 435 Cai, Y., Liu, S., and Lin, H.: Monitoring the Vegetation Dynamics in the Dongting Lake Wetland from 2000 to 2019 Using the BEAST Algorithm Based on Dense Landsat Time Series, *Appl. Sci.*, 10(12), Retrieved from <https://doi.org/10.3390/app10124209>, 2020.
- Chen, Y., Xu, C., Chen, Y., Li, W., and Liu, J.: Response of glacial-lake outburst floods to climate change in the Yarkant River basin on northern slope of Karakoram Mountains, China, *Quat. Int.*, 226(1), 75-81, <https://doi.org/10.1016/j.quaint.2010.01.003>, 2010.

- Clarke, G. K. C.: Fast glacier flow: Ice streams, surging, and tidewater glaciers, *J. Geophys. Res.: Solid Earth*, 92(B9), 8835-8841, <https://doi.org/10.1029/JB092iB09p08835>, 1987.
- Copland, L., Sharp, M. J., and Dowdeswell, J. A.: The distribution and flow characteristics of surge-type glaciers in the Canadian High Arctic, *Ann. Glaciol.*, 36, 73-81, <https://doi.org/10.3189/172756403781816301>, 2003.
- Copland, L., Sylvestre, T., Bishop, M. P., Shroder, J. F., Seong, Y. B., Owen, L. A., Bush, A., and Kamp, U.: Expanded and Recently Increased Glacier Surging in the Karakoram, *Arct. Antarct. Alp. Res.*, 43(4), 503-516, <https://doi.org/10.1657/1938-4246-43.4.503>, 2011.
- Cuffey, K. M. and Paterson, W. S. B. (Eds.): *The physics of glaciers*: Academic Press, 2010.
- Ding, M., Huai, B., Sun, W., Wang, Y., Zhang, D., Guo, X., and Zhang, T.: Surge-type glaciers in Karakoram Mountain and possible catastrophes alongside a portion of the Karakoram Highway, *Nat. Hazards*, 90(2), 1017-1020, <https://doi.org/10.1007/s11069-017-3063-4>, 2018.
- EROS Center: USGS EROS Archive - Digital Elevation - Shuttle Radar Topography Mission (SRTM) 1 Arc-Second Global, <https://doi.org/10.5066/F7PR7TFT>, 2018.
- Farinotti, D., Immerzeel, W. W., de Kok, R. J., Quincey, D. J., and Dehecq, A.: Manifestations and mechanisms of the Karakoram glacier Anomaly, *Nat. Geosci.*, 13(1), 8-16, <https://doi.org/10.1038/s41561-019-0513-5>, 2020.
- Farr, T. G., Rosen, P. A., Caro, E., Crippen, R., Duren, R., Hensley, S., Kobrick, M., Paller, M., Rodriguez, E., Roth, L., Seal, D., Shaffer, S., Shimada, J., Umland, J., Werner, M., Oskin, M., Burbank, D., and Alsdorf, D.: The Shuttle Radar Topography Mission, *Rev. Geophys.*, 45(2), <https://doi.org/10.1029/2005RG000183>, 2007.
- Gardelle, J., Berthier, E., Arnaud, Y., and Käab, A.: Region-wide glacier mass balances over the Pamir-Karakoram-Himalaya during 1999-2011, *The Cryosphere*, 7(4), 1263-1286, <https://doi.org/10.5194/tc-7-1263-2013>, 2013.
- Guillet, G., King, O., Lv, M., Ghuffar, S., Benn, D., Quincey, D., and Bolch, T.: A regionally resolved inventory of High Mountain Asia surge-type glaciers, derived from a multi-factor remote sensing approach, *The Cryosphere*, 16(2), 603-623, <https://doi.org/10.5194/tc-16-603-2022>, 2022.
- Haemmig, C., Huss, M., Keusen, H., Hess, J., Wegmüller, U., Ao, Z., and Kulubayi, W.: Hazard assessment of glacial lake outburst floods from Kyagar glacier, Karakoram mountains, China, *Ann. Glaciol.*, 55(66), 34-44, <https://doi.org/10.3189/2014AoG66A001>, 2014.
- Hewitt, K.: The Karakoram Anomaly? Glacier Expansion and the 'Elevation Effect,' Karakoram Himalaya, *Mt. Res. Dev.*, 25(4), 332-340, 339, [https://doi.org/10.1659/0276-4741\(2005\)025\[0332:TKAGEA\]2.0.CO;2](https://doi.org/10.1659/0276-4741(2005)025[0332:TKAGEA]2.0.CO;2), 2005.
- Hewitt, K. and Liu, J.: Ice-Dammed Lakes and Outburst Floods, Karakoram Himalaya: Historical Perspectives on Emerging Threats, *Phys. Geogr.*, 31(6), 528-551, <https://doi.org/10.2747/0272-3646.31.6.528>, 2010.
- Hugonnet, R., McNabb, R., Berthier, E., Menounos, B., Nuth, C., Girod, L., Farinotti, D., Huss, M., Dussaillant, I., Brun, F., and Käab, A.: Accelerated global glacier mass loss in the early twenty-first century, *Nature*, 592(7856), 726-731, <https://doi.org/10.1038/s41586-021-03436-z>, 2021.

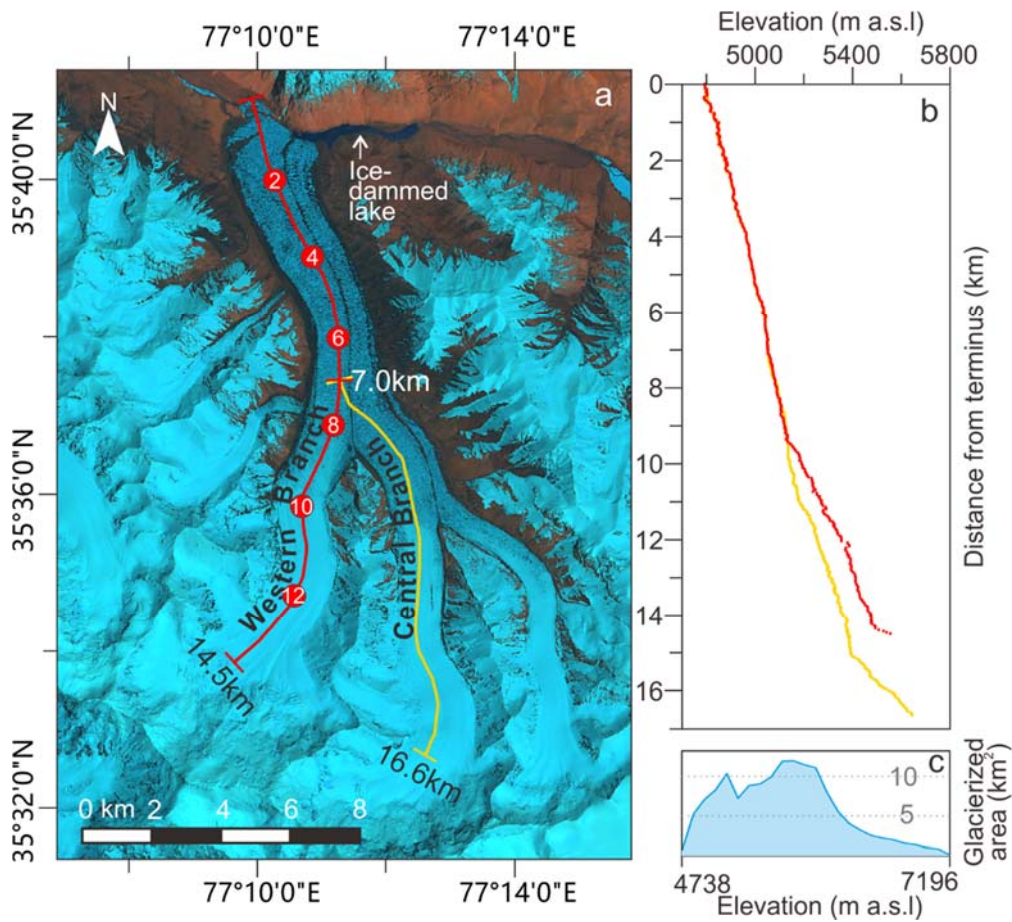
- Jekel, C. F. and Venter, G.: Pwlf: A python library for fitting 1D continuous piecewise linear functions, <http://dx.doi.org/10.13140/RG.2.2.28530.56007>, URL [https://github.com/cjekel/piecewise\\_linear\\_fit\\_py](https://github.com/cjekel/piecewise_linear_fit_py), 2019.
- 475 Jiskoot, H.: *Glacier Surging*, in: *Encyclopedia of Snow, Ice and Glaciers*, edited by: Singh, V. P., Singh, P., and Haritashya, U. K., Springer Netherlands, Dordrecht, 415-428, [https://doi.org/10.1007/978-90-481-2642-2\\_559](https://doi.org/10.1007/978-90-481-2642-2_559), 2011.
- Leprince, S., Barbot, S., Ayoub, F., and Avouac, J.: Automatic and Precise Orthorectification, Coregistration, and Subpixel Correlation of Satellite Images, Application to Ground Deformation Measurements, *IEEE Trans. Geosci. Remote Sens.*, 45(6), 1529-1558, <https://doi.org/10.1109/TGRS.2006.888937>, 2007.
- 480 Lv, M., Guo, H., Lu, X., Liu, G., Yan, S., Ruan, Z., Ding, Y., and Quincey, D. J.: Characterizing the behaviour of surge- and non-surge-type glaciers in the Kingata Mountains, eastern Pamir, from 1999 to 2016, *The Cryosphere*, 13(1), 219-236, <https://doi.org/10.5194/tc-13-219-2019>, 2019.
- Lv, M., Guo, H., Yan, J., Wu, K., Liu, G., Lu, X., Ruan, Z., and Yan, S.: Distinguishing Glaciers between Surging and Advancing by Remote Sensing: A Case Study in the Eastern Karakoram, *Remote Sens.*, 12(14), 2297, <https://doi.org/10.3390/rs12142297>, 2020a.
- 485 Lv, M., Quincey, D. J., Guo, H., King, O., Liu, G., Yan, S., Lu, X., and Ruan, Z.: Examining geodetic glacier mass balance in the eastern Pamir transition zone, *J. Glaciol.*, 1-11, <https://doi.org/10.1017/jog.2020.54>, 2020b.
- Markham, B. L., Storey, J. C., Williams, D. L., and Irons, J. R.: Landsat sensor performance: history and current status, *IEEE Trans. Geosci. Remote Sens.*, 42, 2691-2694, <https://doi.org/10.1109/TGRS.2004.840720>, 2004.
- 490 Mastrandrea, M. D., Field, C. B., Stocker, T. F., Edenhofer, O., Ebi, K. L., Frame, D. J., Held, H., Kriegler, E., Mach, K. J., and Matschoss, P. R.: *Guidance note for lead authors of the IPCC fifth assessment report on consistent treatment of uncertainties*, 2010.
- NASA/METI/AIST/Japan Spacesystems and U.S./Japan ASTER Science Team: ASTER DEM Product [Data set], NASA EOSDIS Land Processes DAAC, <https://doi.org/10.5067/ASTER/AST14DEM.003>, 2001. Date Accessed 12-06-2022
- 495 Nuth, C. and Kääb, A.: Co-registration and bias corrections of satellite elevation data sets for quantifying glacier thickness change, *The Cryosphere*, 5(1), 271-290, <https://doi.org/10.5194/tc-5-271-2011>, 2011.
- Paul, F.: A 60-year chronology of glacier surges in the central Karakoram from the analysis of satellite image time-series, *Geomorphology*, 352, 106993, <https://doi.org/10.1016/j.geomorph.2019.106993>, 2020.
- 500 Pitte, P., Berthier, E., Masiokas, M. H., Cabot, V., Ruiz, L., Ferri Hidalgo, L., Gargantini, H., and Zalazar, L.: *Geometric evolution of the Horcones Inferior Glacier (Mount Aconcagua, Central Andes) during the 2002–2006 surge*, *J. Geophys. Res.: Earth Surface*, 121, 111-127, <https://doi.org/10.1002/2015JF003522>, 2016.
- Ragetli, S., Bolch, T., and Pellicciotti, F.: Heterogeneous glacier thinning patterns over the last 40 years in Langtang Himal, Nepal, *The Cryosphere*, 10(5), 2075-2097, <https://doi.org/10.5194/tc-10-2075-2016>, 2016.
- 505 Rashid, I., Majeed, U., Jan, A., and Glasser, N. F.: The January 2018 to September 2019 surge of Shisper Glacier, Pakistan, detected from remote sensing observations, *Geomorphology*, 351, 106957, <https://doi.org/10.1016/j.geomorph.2019.106957>, 2020.

- Rignot, E., Echelmeyer, K., and Krabill, W.: Penetration depth of interferometric synthetic-aperture radar signals in snow and ice, *Geophys. Res. Lett.*, 28(18), 3501-3504, <https://doi.org/10.1029/2000GL012484>, 2001.
- Round, V., Leinss, S., Huss, M., Haemmig, C., and Hajnsek, I.: Surge dynamics and lake outbursts of Kyagar Glacier, Karakoram, *The Cryosphere*, 11(2), 723-739, <https://doi.org/10.5194/tc-11-723-2017>, 2017.
- 510 Sevestre, H. and Benn, D. I.: Climatic and geometric controls on the global distribution of surge-type glaciers: implications for a unifying model of surging, *J. Glaciol.*, 61(228), 646-662, <https://doi.org/10.3189/2015JoG14J136>, 2015.
- Shangguan, D., Liu, S., Ding, Y., Guo, W., Xu, B., Xu, J., and Jiang, Z.: Characterizing the May 2015 Karayaylak Glacier surge in the eastern Pamir Plateau using remote sensing, *J. Glaciol.*, 62(235), 944-953, <https://doi.org/10.1017/jog.2016.81>, 2016.
- 515 Shean, D. E.: *High Mountain Asia 8-meter DEMs Derived from Along-track Optical Imagery, Version 1*, Boulder, Colorado USA, NASA National Snow and Ice Data Center Distributed Active Archive Center, <https://doi.org/10.5067/GSACB044M4PK>, 2017a. Date Accessed 12-06-2022
- Shean, D. E.: *High Mountain Asia 8-meter DEMs Derived from Cross-track Optical Imagery, Version 1*, Boulder, Colorado USA, NASA National Snow and Ice Data Center Distributed Active Archive Center, <https://doi.org/10.5067/0MCWJJH5ABYO>, 2017b. Date Accessed 12-06-2022
- 520 Shean, D. E., Alexandrov, O., Moratto, Z. M., Smith, B. E., Joughin, I. R., Porter, C., and Morin, P.: An automated, open-source pipeline for mass production of digital elevation models (DEMs) from very-high-resolution commercial stereo satellite imagery, *ISPRS J. Photogramm. Remote Sens.*, 116, 101-117, <https://doi.org/10.1016/j.isprsjprs.2016.03.012>, 2016.
- Shi, Y. and Liu, S.: Estimation on the response of glaciers in China to the global warming in the 21st century, *Chinese Science Bulletin*, 45, 668-672, <https://doi.org/10.1007/BF02886048>, 2000.
- 525 Storn, R. and Price, K. V.: Differential Evolution – A Simple and Efficient Heuristic for global Optimization over Continuous Spaces, *J. Glob. Optim.*, 11, 341-359, <https://doi.org/10.1023/A:1008202821328>, 1997.
- Thayyen, R. J. and Gergan, J. T.: Role of glaciers in watershed hydrology: a preliminary study of a "Himalayan catchment", *The Cryosphere*, 4, 115-128, <https://doi.org/10.5194/tc-4-115-2010>, 2010.
- 530 Truffer, M., Kääb, A., Harrison, W. D., Osipova, G. B., Nosenko, G. A., Espizua, L., Gilbert, A., Fischer, L., Huggel, C., Crawford, P. A., and Lai, A. W.: Chapter 13 - Glacier surges, in: *Snow and Ice-Related Hazards, Risks, and Disasters (Second Edition)*, edited by: Haerberli, W., and Whiteman, C., Elsevier, 417-466, <https://doi.org/10.1016/B978-0-12-817129-5.00003-2>, 2021.
- 535 Wei, R.-j., Peng, L., Liang, C., Haemmig, C., Huss, M., Mu, Z.-x., and He, Y.: Analysis of temporal and spatial variations in hydrometeorological elements in the Yarkant River Basin, China, *J. Water Clim. Change*, 10(1), 167-180, <https://doi.org/10.2166/wcc.2018.111>, 2018.
- Wulder, M. A., Roy, D. P., Radeloff, V. C., Loveland, T. R., Anderson, M. C., Johnson, D. M., Healey, S., Zhu, Z., Scambos, T. A., Pahlevan, N., Hansen, M., Gorelick, N., Crawford, C. J., Masek, J. G., Hermosilla, T., White, J. C., Belward, A. S., Schaaf, C., Woodcock, C. E., Huntington, J. L., Lymburner, L., Hostert, P., Gao, F., Lyapustin, A., Pekel, J.-F., Strobl, P.,

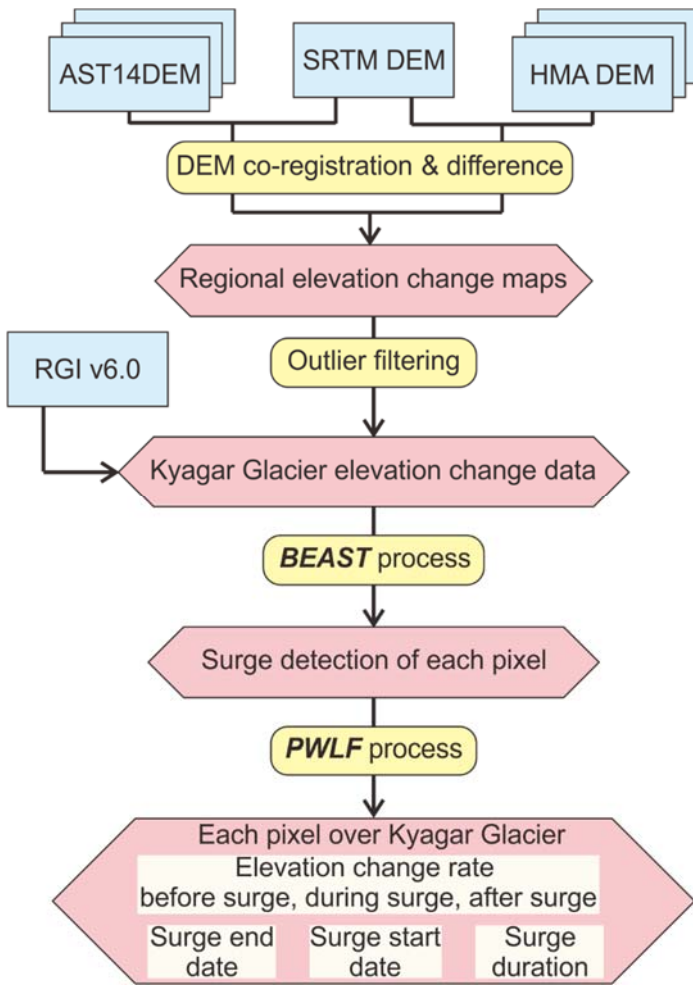
- 540 and Cook, B. D.: Fifty years of Landsat science and impacts, *Remote Sens. Environ.*, 280, 113195, <https://doi.org/10.1016/j.rse.2022.113195>, 2022.
- Yin, B., Zeng, J., Zhang, Y., Huai, B., and Wang, Y.: Recent Kyagar glacier lake outburst flood frequency in Chinese Karakoram unprecedented over the last two centuries, *Nat. Hazards*, 95(3), 877-881, <https://doi.org/10.1007/s11069-018-3505-7>, 2019.
- 545 Zhang, M., Chen, F., Tian, B., Liang, D., and Yang, A.: Characterization of Kyagar Glacier and Lake Outburst Floods in 2018 Based on Time-Series Sentinel-1A Data, *Water*, 12(1), <https://doi.org/10.3390/w12010184>, 2020.
- Zhang, X.: Investigation of glacier bursts of the Yarkant River in Xinjiang, China, *Ann. Glaciol.*, 16, 135-139, <https://doi.org/10.3189/1992AoG16-1-135-139>, 1992.
- Zhang, Z., Zhao, J., Liu, S., Zhang, Q., Jiang, Z., Xu, Y., and Hu, K.: Characterization of Three Surges of the Kyagar Glacier, Karakoram, *SSRN*, <http://dx.doi.org/10.2139/ssrn.4065221>, 2022.
- 550 Zhao, K., Wulder, M. A., Hu, T., Bright, R., Wu, Q., Qin, H., Li, Y., Toman, E., Mallick, B., Zhang, X., and Brown, M.: Detecting change-point, trend, and seasonality in satellite time series data to track abrupt changes and nonlinear dynamics: A Bayesian ensemble algorithm, *Remote Sens. Environ.*, 232, 111181, <https://doi.org/10.1016/j.rse.2019.04.034>, 2019.



555 Figure 1. Location of the Kyagar Glacier and regional geographical conditions. Labelled Mount Chogori is to assist orientation. The background is Landsat OLI image (band 6-5-4) acquired on 6 September 2021.



560 Figure 2: (a) Location of the ice-dammed lake and elevation profiles of the Kyagar Glacier. The background is a sharpened Landsat OLI image (band 6-5-4) acquired on 4 July 2015. Red dots indicate points along the western branch in Figure 6 and 8. (b) Elevation along two centerlines from the terminus; the western branch is shown in red and the central branch shown in yellow. (c) Hypsometry curve of Kyagar Glacier.



565

Figure 3: Workflow to quantify glacial behaviour using multi-temporal DEMs

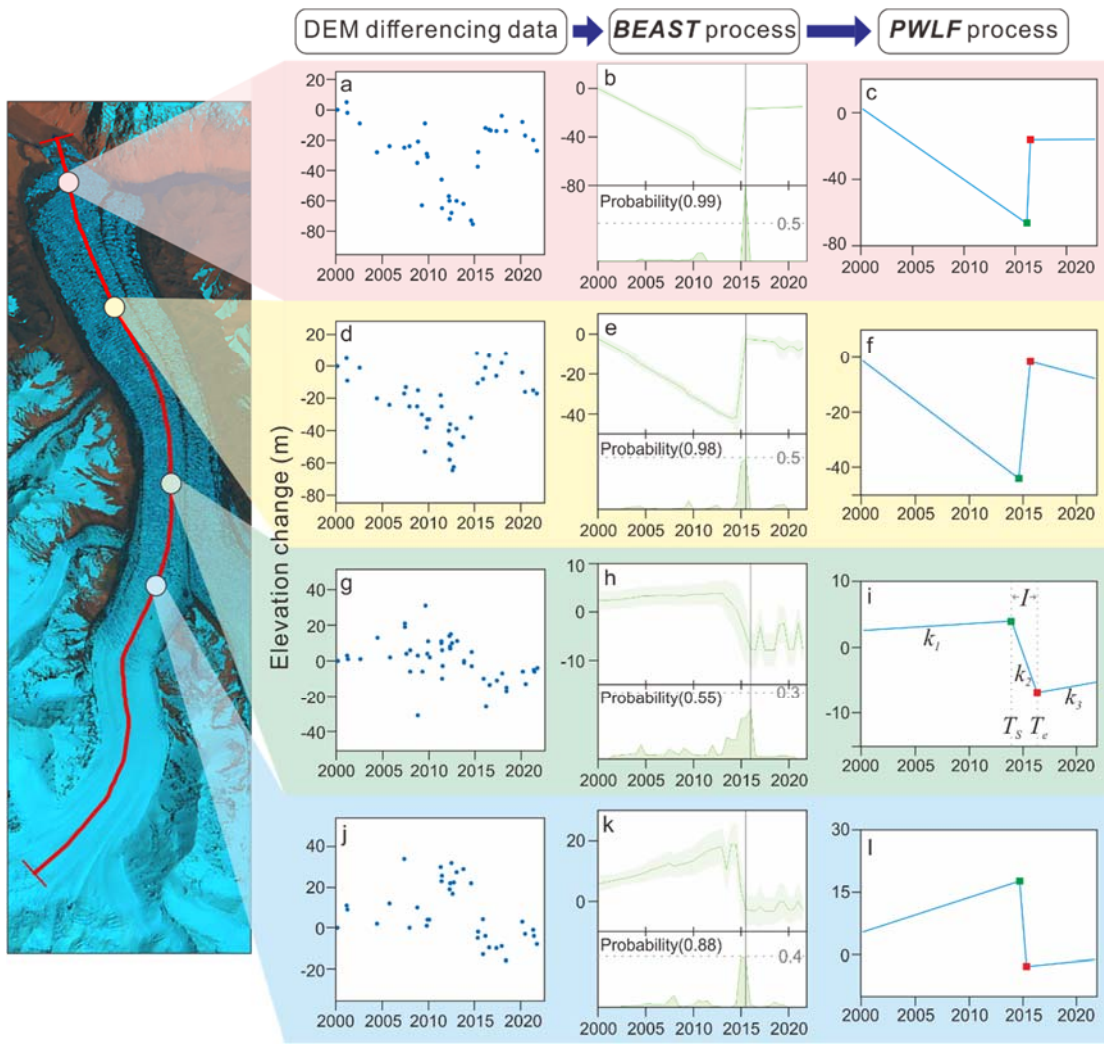


Figure 4: Presentation of DEM differencing data post-processing. Four random pixels were selected along the central profile of the western branch. The green spots in c, f, i, and l represented the timing of each pixel starting to endure surge impact. The red spots represented the end of surge impact on each pixel. Parameters identified in i are shown in Figure 810.

570

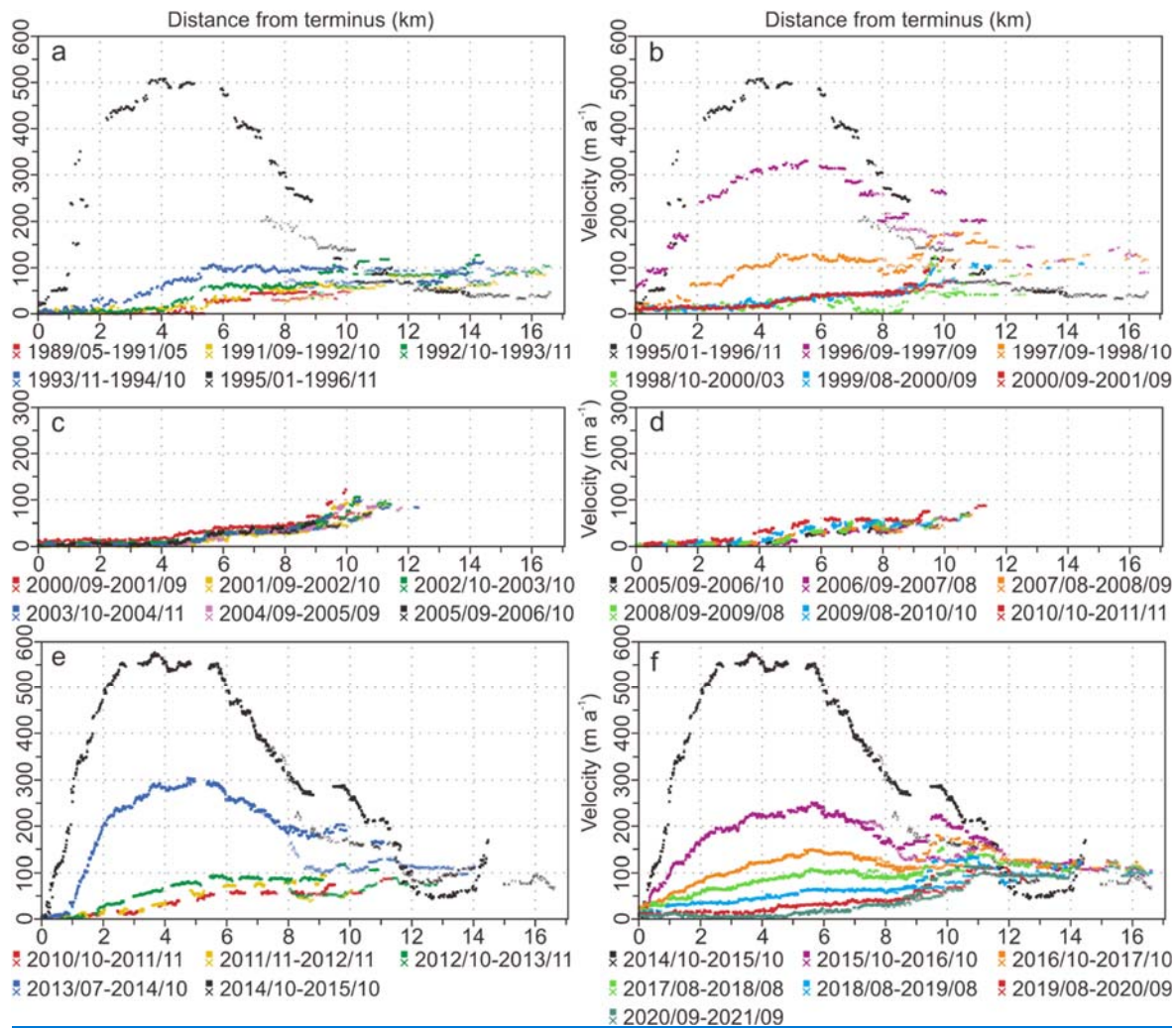
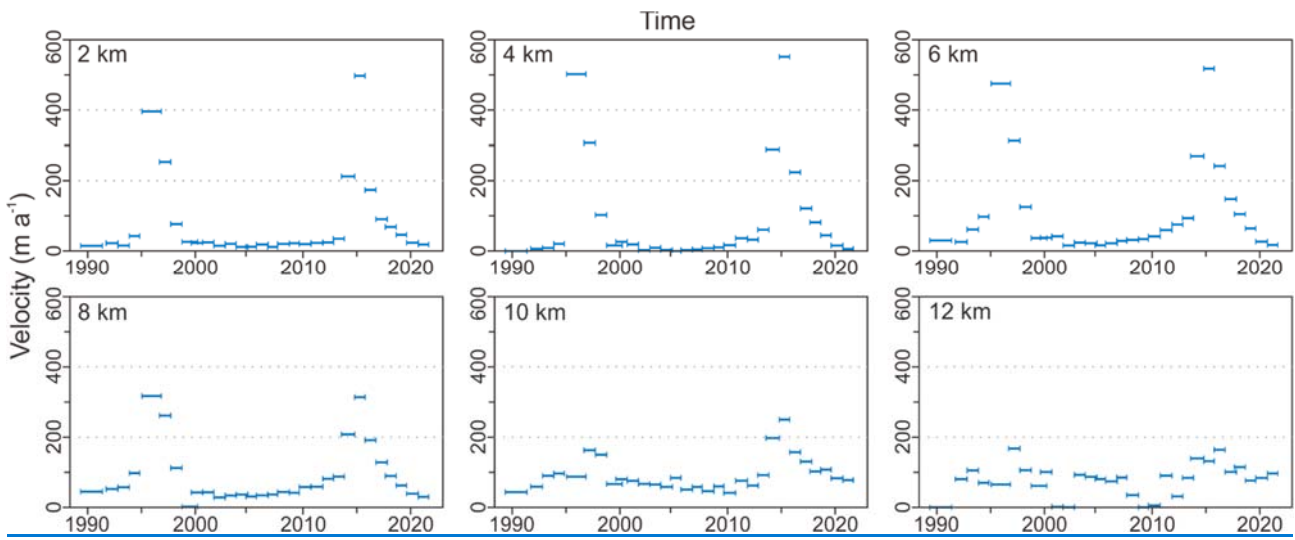
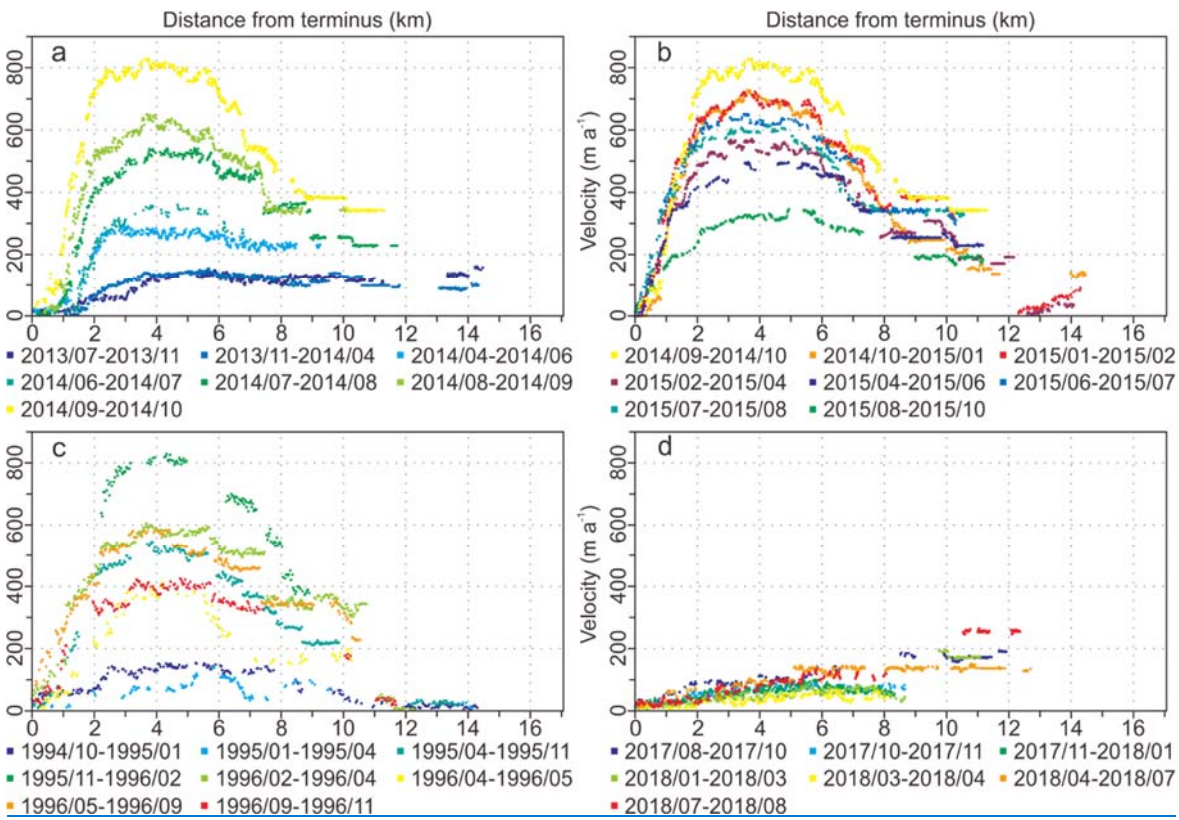


Figure 5: Annual velocity profiles along the western and central branches of Kyagar Glacier from 1989 to 2021. The centerline of the western branch is formed by square dots and the centerline of the central branch is formed by crosses.

575



**Figure 6:** Annual velocities of different points along the western branch of Kyagar Glacier from 1989 to 2021. The points are shown in Figure 2a and selected at 2, 4, 6, 8, 10, 12 km from the terminus.



**Figure 7:** Near monthly velocity profiles along western branch centerline of Kyagar Glacier during two surging periods.

580

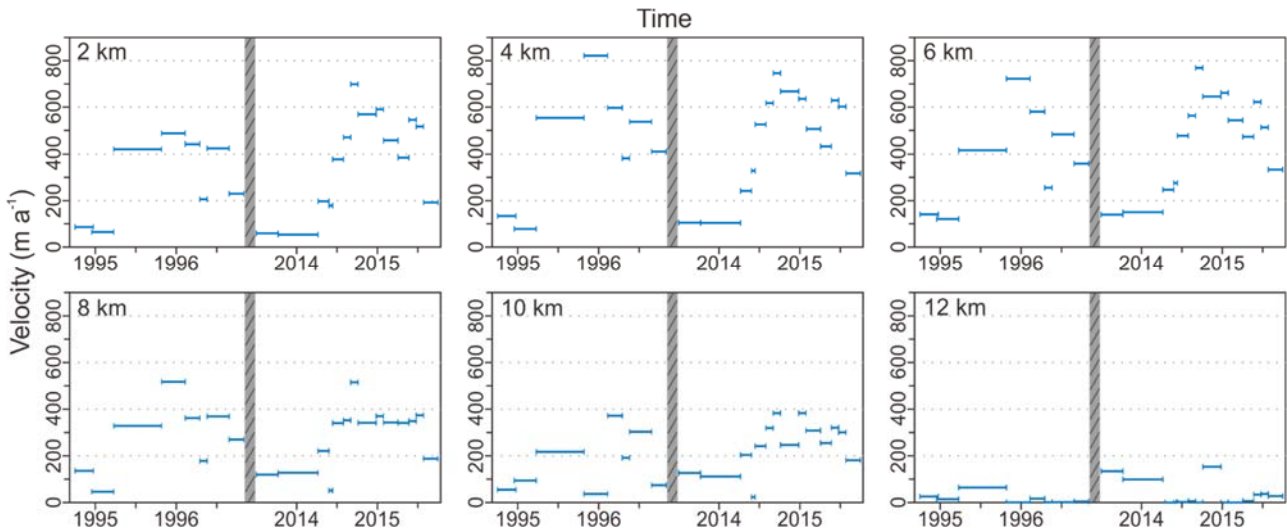


**Figure 8:** Near monthly velocities of different points along the western branch of Kyagar Glacier during two surging periods. The points are shown in Figure 2a and selected at 2, 4, 6, 8, 10, 12 km from the terminus.

585

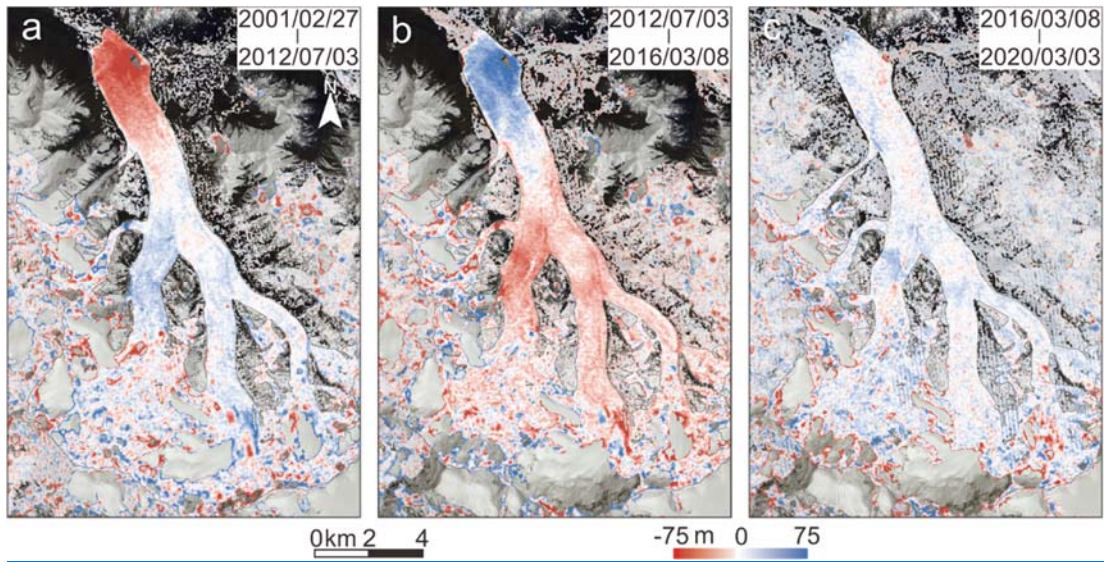
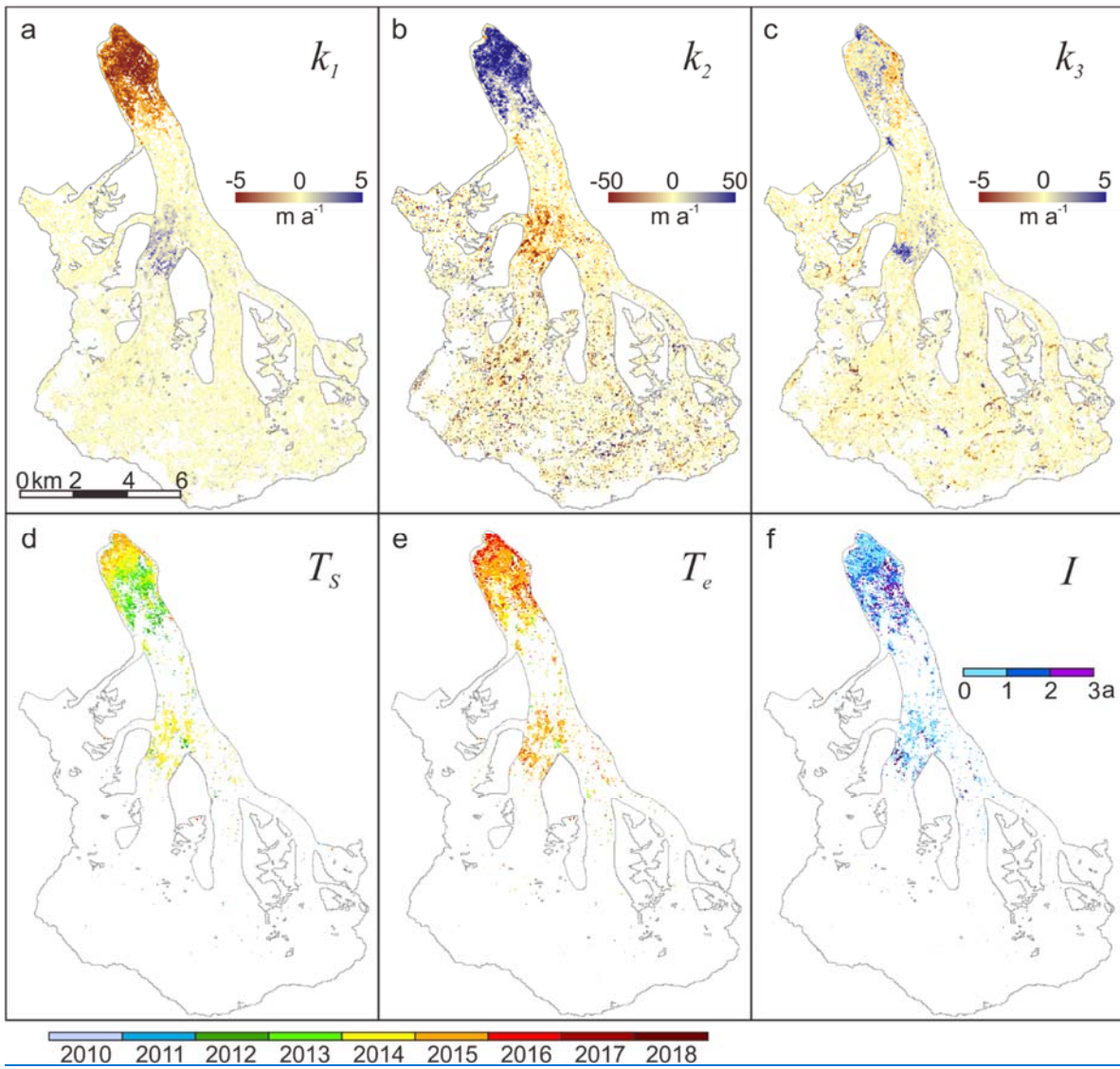
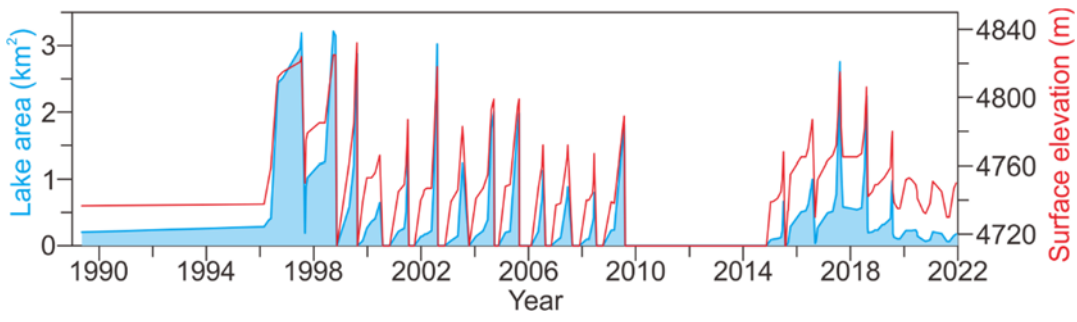


**Figure 9:** Surface elevation changes of Kyagar Glacier during three periods (a: 2001 - 2012, b: 2012 - 2016, c: 2016 - 2020).



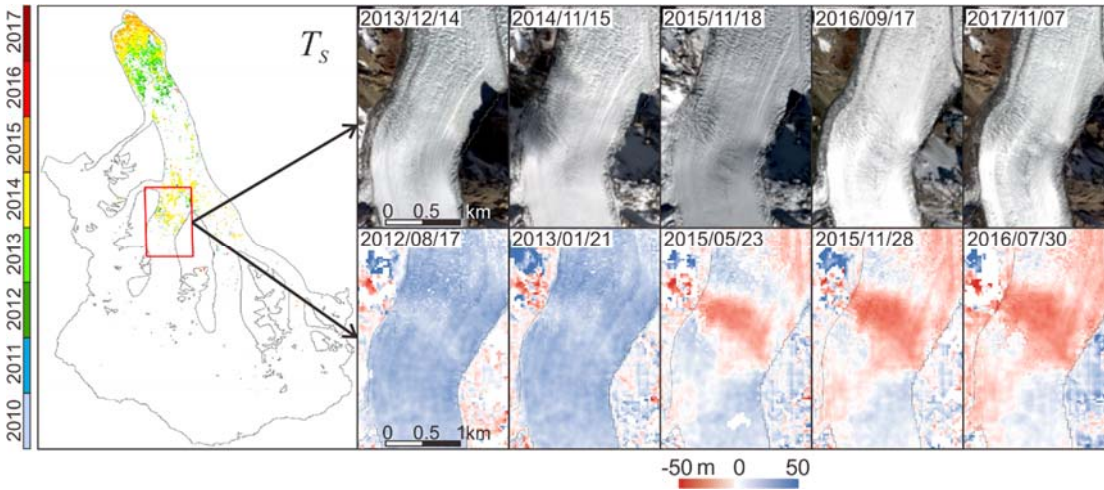
590

**Figure 810:** Parameter maps quantifying elevation changes of Kyagar Glacier. Elevation-change rates before, during, and after the surge of each pixel are labeled as  $k_1$ ,  $k_2$ , and  $k_3$ .  $T_s$  and  $T_e$  represent the dates of surge impact initiated and terminated on each pixel.  $I$  represents the duration of surge impact.



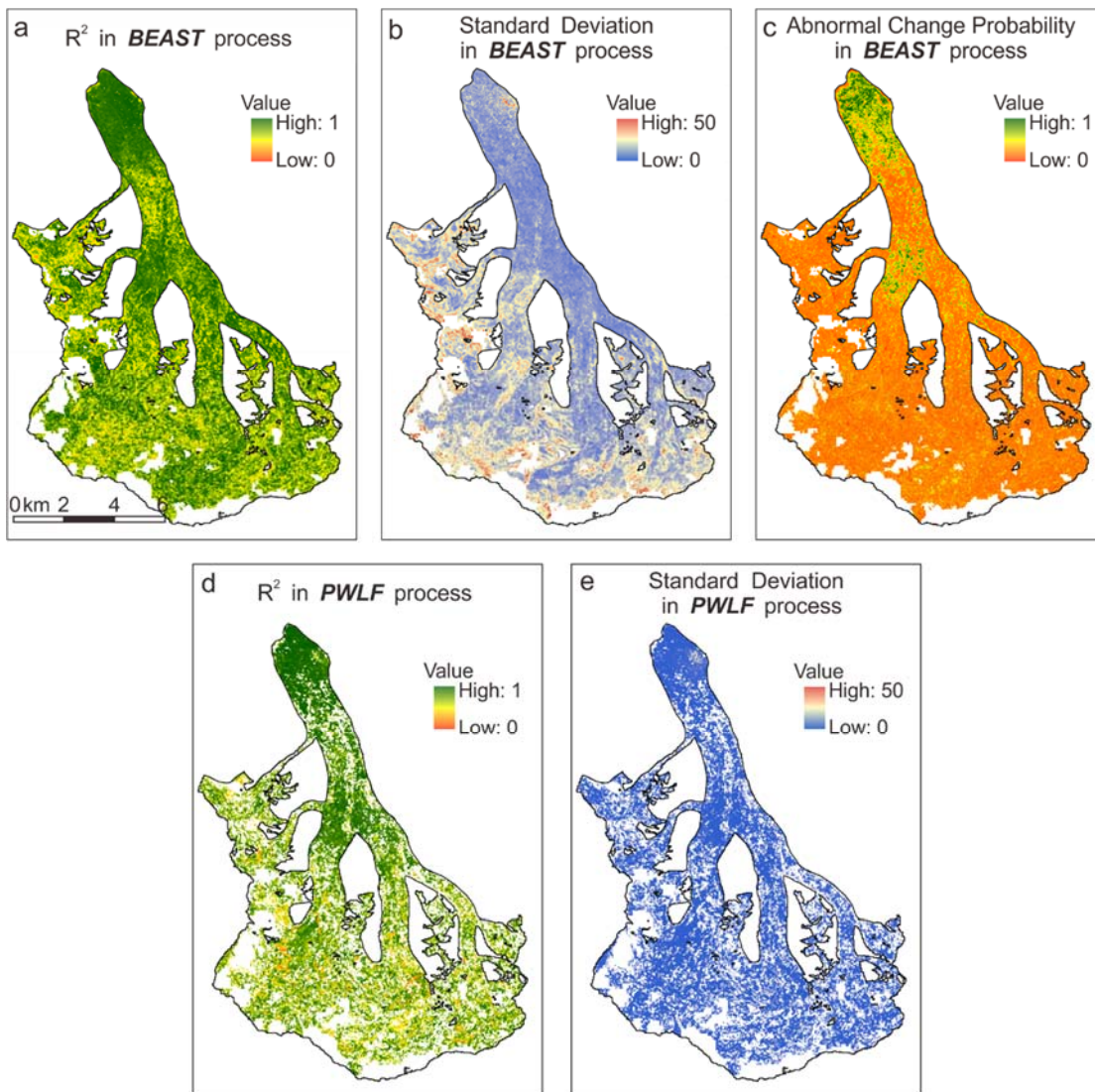
595

Figure 911: Evolution of ice-dammed lake surface elevation and area from 1989 to 2021.



600

Figure 1012: Details of Landsat 8 OLI images and elevation changes over reservoir zone. Elevation changes between HMA DEM and SRTM DEM are shown.



605 **Figure 413:**  $R^2$  (a), standard deviation (b), and abnormal change probability (c) in BEAST process;  $R^2$  (d) and standard deviation (e) in PWLF process.

**Table 1: Details of the Landsat series images and DEMs used in this study**

Product/Sensor	Resolution (m)	Date of acquisition	Scenes
<b>DEMs</b>			
ASTER DEM	30	2001 Feb 27 – 2021 Sep 30	67
HMA DEM	8	2011 Jun 25 – 2016 Oct 2	17
SRTM DEM	<del>30</del> ~90	2000 Feb 11-22	1
<b>Landsat imagery</b>			

Landsat-5 TM	30	1989 Aug 6 – 2000 Mar 20	85
Landsat-7 ETM+	30/15(band 8)	1999 Jul 25 – 2013 May 19	147
Landsat-8 OLI	30/15(band 8)	2013 Jun 5 – 2021 Dec 11	141

---

**Table S1.** Mean differences and the standard deviation (SD) of elevation difference maps over off-glacier areas before and after co-registration process.

DEM Product ID	Date	Statistics of stable ground differences (Product vs SRTM) (m)			
		Pre-mean	Pre-SD	Post-mean	Post-SD
AST14DEM_00302272001055811	2001/2/27		10.547		
AST14DEM_00303312001055714	2001/3/31	5.8334	6	-0.3708	10.1930
AST14DEM_00304252001055043	2001/4/25	10.609.81	2.63	1.660.67	19
AST14DEM_00308022002054207	2002/8/2	33.7919	0.55	1.8920	21.46
AST14DEM_00305082003054658	2003/5/8	6.3614	3	0.8668	10.5674
AST14DEM_00305032004054046	2004/5/3	10.4044	7.89	0.3115	39.5634
AST14DEM_00305032004054037	2004/5/3	5.096.36	8.78	2.081.56	29
AST14DEM_00306112004054637	2004/6/11	7.1311	5	1.9171	12.2707
AST14DEM_00310202005054549	2005/10/20	2.5711	6	-0.1538	93
AST14DEM_00311142005053944	2005/11/14	-2.3396	1.45	0.6614	9.9558
AST14DEM_00311142005053953	2005/11/14	25.9824.8	24.192	2.181.06	24.1322.
AST14DEM_00311302005053951	2005/11/30	6	2.21	3.421.45	32
AST14DEM_00302092006054532	2006/2/9	32.0025.2	21.462	4.911.83	31.5421.
AST14DEM_00305282007054024	2007/5/28	4	7.54	77	26.8716.
AST14DEM_00305282007054033	2007/5/28	28.5020.1	25.231	-	-
AST14DEM_00307312007054050	2007/7/31	4	7.15	18.748	15.1628
AST14DEM_00307312007054059	2007/7/31	14.7415.2	18.748	0.5500	15.1628
AST14DEM_00312222007054044	2007/12/22	9	4	1.8775	11.1123
AST14DEM_00312222007054035	2007/12/22	6.9571	0	1.4520	86
AST14DEM_00312222008054024	2008/3/11	19.151	34.162	1.4737	60
AST14DEM_00310212008054055	2008/10/21	3.822.53	7.41	2.911.93	56
AST14DEM_00310212008054046	2008/10/21	13.106.90	9.90	2.320.82	80
AST14DEM_00311222008054054	2008/11/22	7.166.46	6.46	0.6431	12.5630
AST14DEM_00311222008054103	2008/11/22	27.502	27.502	15.747	14.4764
AST14DEM_00304222009054745	2009/4/22	7.166.46	6.46	0.2503	3

AST14DEM_00308212009054049	2009/8/21		24.762		25.4724
		14.3417	3	1.4724	45
AST14DEM_00310312009054651	2009/10/31		12.053		
		-2.873.46	9	-0.0354	12.0336
AST14DEM_00312022009054657	2009/12/2		10.548		
		-6.1168	4	-0.2923	10.1622
AST14DEM_00302042010054646	2010/2/4		14.405		13.0412
		2.9340	7	-0.2223	96
AST14DEM_00304092010054648	2010/4/9		11.455		
		0.4103	2	-0.2316	11.1923
AST14DEM_00309162010054631	2010/9/16		17.590		
		-7.548.04	4	-0.3613	12.6049
AST14DEM_00301312011054004	2011/1/31		36.384		
		1.230.92	8	1.1277	36.2112
AST14DEM_00305072011054026	2011/5/7		15.986		
		-0.0548	2	1.4001	11.3847
AST14DEM_00305072011054035	2011/5/7		16.691		
		-1.232.42	5.77	1.0506	11.2841
AST14DEM_00306082011054011	2011/6/8		16.913		
		2.021.83	5	0.5750	10.4875
AST14DEM_00306082011054020	2011/6/8		20.461		12.6811
		-1.762.75	8.02	0.6656	64
AST14DEM_00306242011054010	2011/6/24		11.041		
		7.5234	0.86	0.431.29	9.7587
AST14DEM_00306242011054019	2011/6/24		13.471		12.2511
		4.86 6.05	2.41	0.4233	58
AST14DEM_00303222012054024	2012/3/22		18.581		
		16.7538	7.56	1.080.76	15.7625
AST14DEM_00304142012054630	2012/4/14		12.001		
		4.44 5.09	1.84	-0.0141	11.9879
AST14DEM_00304232012054026	2012/4/23		25.852		18.7716
		24.9370	3.33	0.561.03	94
AST14DEM_00304232012054035	2012/4/23		26.472		18.0014
		22.3419.8	2.19	1.610.35	93
AST14DEM_00305092012054029	2012/5/9		15.371		14.4213
		22.0821.5	4.29	1.380.77	97
AST14DEM_00305162012054638	2012/5/16		12.414		
		-3.3495	0	0.3780	12.4129
AST14DEM_00307032012054636	2012/7/3		20.881		
		2.251.64	9.03	0.8340	13.6105
AST14DEM_00310192013054017	2013/10/19		26.292		26.2625
		10.429.86	5.58	1.7312	53
AST14DEM_00310192013054025	2013/10/19		32.002		32.6126
		9.615.59	7.38	1.920.90	71
AST14DEM_00308192014054100	2014/8/19		13.311		
		3.182.97	1	1.2801	11.2809
AST14DEM_00308192014054109	2014/8/19		16.421		13.6712
		-3.944.98	4.77	0.2428	40
AST14DEM_00302112015054102	2015/2/11		22.802		22.5820
		0.33-2.36	1.49	2.171.39	93
AST14DEM_00309142015054723	2015/9/14		12.472		11.0110
		-2.0057	5	-0.3801	97
AST14DEM_00312032015054715	2015/12/3		-		
		16.5017.0	16.773		
		6	3	-0.1538	14.2308

AST14DEM_00303082016054644	2016/3/8	-	<u>15.7816.3</u>	<u>12.986</u>		
			<u>1</u>	<u>2</u>	<u>-0.1331</u>	<u>11.1600</u>
AST14DEM_00303242016054647	2016/3/24			<u>11.141</u>		
		<u>-4.815.15</u>	<u>6</u>		<u>-0.1750</u>	<u>10.2943</u>
AST14DEM_00305142017054652	2017/5/14			<u>16.581</u>		
		<u>-4.655.32</u>	<u>5.79</u>		<u>0.681.04</u>	<u>13.5202</u>
AST14DEM_00305302017054652	2017/5/30			<u>25.142</u>		<u>23.4619.</u>
		<u>2.480.33</u>	<u>0.98</u>		<u>1.480.40</u>	<u>87</u>
AST14DEM_00312082017054653	2017/12/8			<u>11.051</u>		
		<u>-1.2081</u>	<u>0.84</u>		<u>0.6201</u>	<u>10.6242</u>
AST14DEM_00305262018054155	2018/5/26		<u>23.4822.8</u>	<u>27.182</u>		<u>16.2914.</u>
		<u>7</u>	<u>4.62</u>		<u>1.1413</u>	<u>22</u>
AST14DEM_00305262018054204	2018/5/26			<u>37.112</u>		<u>27.2716.</u>
		<u>14.9589</u>	<u>7.46</u>		<u>2.150.71</u>	<u>47</u>
AST14DEM_00305292019054059	2019/5/29			<u>20.111</u>		<u>13.3112.</u>
		<u>-0.591.98</u>	<u>8.08</u>		<u>1.7820</u>	<u>09</u>
AST14DEM_00305292019054050	2019/5/29			<u>16.350</u>		
		<u>2.8063</u>	<u>5</u>		<u>0.9888</u>	<u>11.2948</u>
AST14DEM_00303032020054720	2020/3/3			<u>16.321</u>		<u>15.5014.</u>
		<u>-6.988.20</u>	<u>4.70</u>		<u>0.50</u>	<u>35</u>
AST14DEM_00306232020054643	2020/6/23			<u>21.382</u>		
		<u>1.6114</u>	<u>0.40</u>		<u>0.4202</u>	<u>14.60</u>
AST14DEM_00305092021054453	2021/5/9			<u>23.642</u>		<u>19.1617.</u>
		<u>2.231.55</u>	<u>1.98</u>		<u>0.69</u>	<u>1.38</u>
AST14DEM_00306032021053822	2021/6/3		<u>17.2116.5</u>	<u>30.012</u>		<u>16.0814.</u>
		<u>7</u>	<u>8.27</u>		<u>1.6528</u>	<u>69</u>
AST14DEM_00306032021053813	2021/6/3			<u>22.975</u>		
		<u>20.4022</u>	<u>4</u>		<u>1.6943</u>	<u>12.7748</u>
AST14DEM_00309302021054225	2021/9/30			<u>20.551</u>		
		<u>7.326.90</u>	<u>9.68</u>		<u>-0.2904</u>	<u>11.7782</u>
HMA_DEM8m_AT_20110625_0602_103 001000B995100_103001000B62DE00	2011/6/25			<u>6.0368</u>	<u>0.2216</u>	<u>5.796.30</u>
		<u>-21.3973</u>		<u>5.806.3</u>		
HMA_DEM8m_AT_20110625_0602_103 001000C6D7F00_103001000B48A500	2011/6/25			<u>8</u>	<u>0.4411</u>	<u>5.5295</u>
		<u>-18.5374</u>				
HMA_DEM8m_AT_20120817_0555_103 001001ABA5800_103001001BA72400	2012/8/17		<u>17.3818.0</u>	<u>5.676.3</u>		
		<u>2</u>	<u>0</u>		<u>0.1507</u>	<u>6.055.54.</u>
HMA_DEM8m_AT_20121002_0548_102 001001D519C00_102001001E5C8700	2012/10/2			<u>6.1184</u>	<u>0.2213</u>	<u>6.0259</u>
		<u>-14.1060</u>				
HMA_DEM8m_AT_20130121_0537_102 001001E3AD500_102001001FD84200	2013/1/21			<u>6.1082</u>	<u>0.3231</u>	<u>5.926.53</u>
		<u>-17.3177</u>				
HMA_DEM8m_AT_20150321_0533_104 001000970E100_1040010009200000	2015/3/21			<u>6.08</u>	<u>0.23</u>	<u>5.67</u>
		<u>-18.94</u>				
HMA_DEM8m_AT_20150409_0533_104 001000A61D300_104001000A3BBC00	2015/4/9			<u>5.586.0</u>		
		<u>-17.3271</u>	<u>7</u>		<u>0.2825</u>	<u>5.4281</u>
HMA_DEM8m_AT_20150409_0534_104 001000A8D7900_104001000955A900	2015/4/9			<u>5.0955</u>	<u>0.2017</u>	<u>5.0033</u>
		<u>-17.5365</u>				
HMA_DEM8m_AT_20150507_0542_105 0410012A5C000_1050410012A5BF00	2015/5/7		<u>18.7119.0</u>			
		<u>5</u>	<u>6.3097</u>		<u>0.2014</u>	<u>5.846.33</u>
HMA_DEM8m_AT_20150523_0550_103 0010042AEB200_103001004177F700	2015/5/23			<u>5.526.0</u>		
		<u>22.8523.1</u>	<u>4</u>	<u>9</u>	<u>0.1109</u>	<u>5.3881</u>
HMA_DEM8m_AT_20151016_0545_104 0010012C70E00_104001001380D500	2015/10/16			<u>5.756.3</u>		
		<u>-16.5788</u>	<u>4</u>		<u>0.2622</u>	<u>5.3579</u>

HMA_DEM8m_AT_20151128_0742_102 00100481CBF00_10200100470C5800	2015/11/28	- <del>19.96</del> <u>21.6</u>	<del>7.63</del> <u>8.1</u>	-0.03 <u>07</u>	<u>7.38</u> <u>56</u>
HMA_DEM8m_AT_20160730_0547_103 0010058028600_103001005A695500	2016/7/30	- <del>18.66</del> <u>19.0</u>	<del>5.70</del> <u>6.3</u>	0.15 <u>13</u>	<u>5.55</u> <u>6.10</u>
HMA_DEM8m_AT_20161002_0535_105 0010006818700_1050010006818900	2016/10/2	- <del>17.75</del> <u>18.0</u>	<del>5.41</del> <u>97</u>	0.10 <u>04</u>	<u>5.13</u> <u>54</u>
HMA_DEM8m_AT_20161002_0534_105 0010006818800_1050010006818600	2016/10/2	-19.26	6.36	0.23	5.79
HMA_DEM8m_CT_20141025_1736_104 0010003AC5200_10300100388CC800	2014/10/25	- <del>11.83</del> <u>12.4</u>	<del>6.61</del> <u>81</u>	0.02 <u>09</u>	<u>6.50</u> <u>57</u>
HMA_DEM8m_CT_20141129_1801_103 001003CC3F400_1020010038C4A900	2014/11/29	- <del>17.98</del> <u>18.4</u>	<del>6.11</del> <u>56</u>	0.20 <u>18</u>	<u>5.83</u> <u>6.12</u>

**Figure S1.** Sharpened Landsat images showing ice-dammed lake evolution (1).

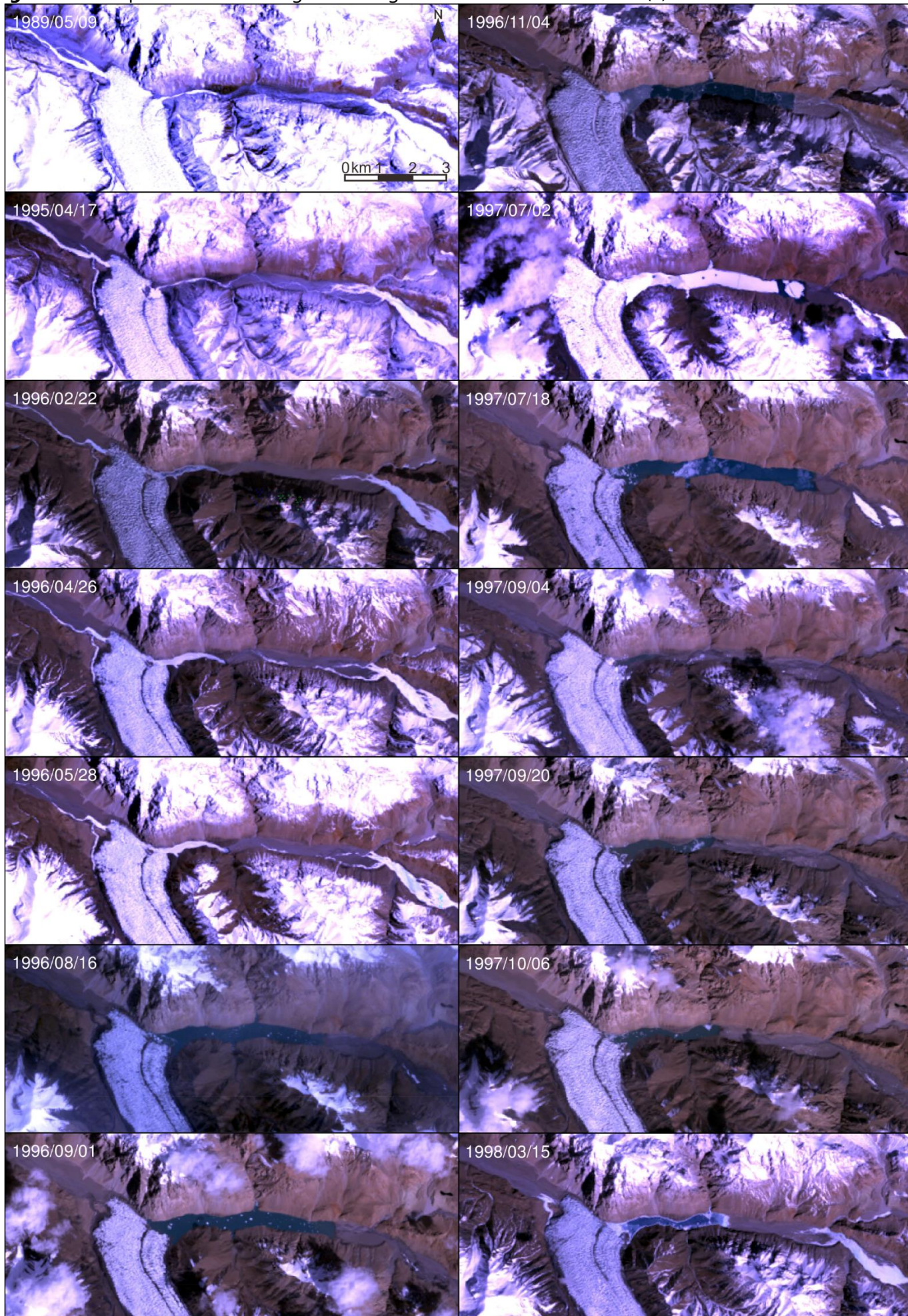


**Figure S2.** Sharpened Landsat images showing ice-dammed lake evolution (2).

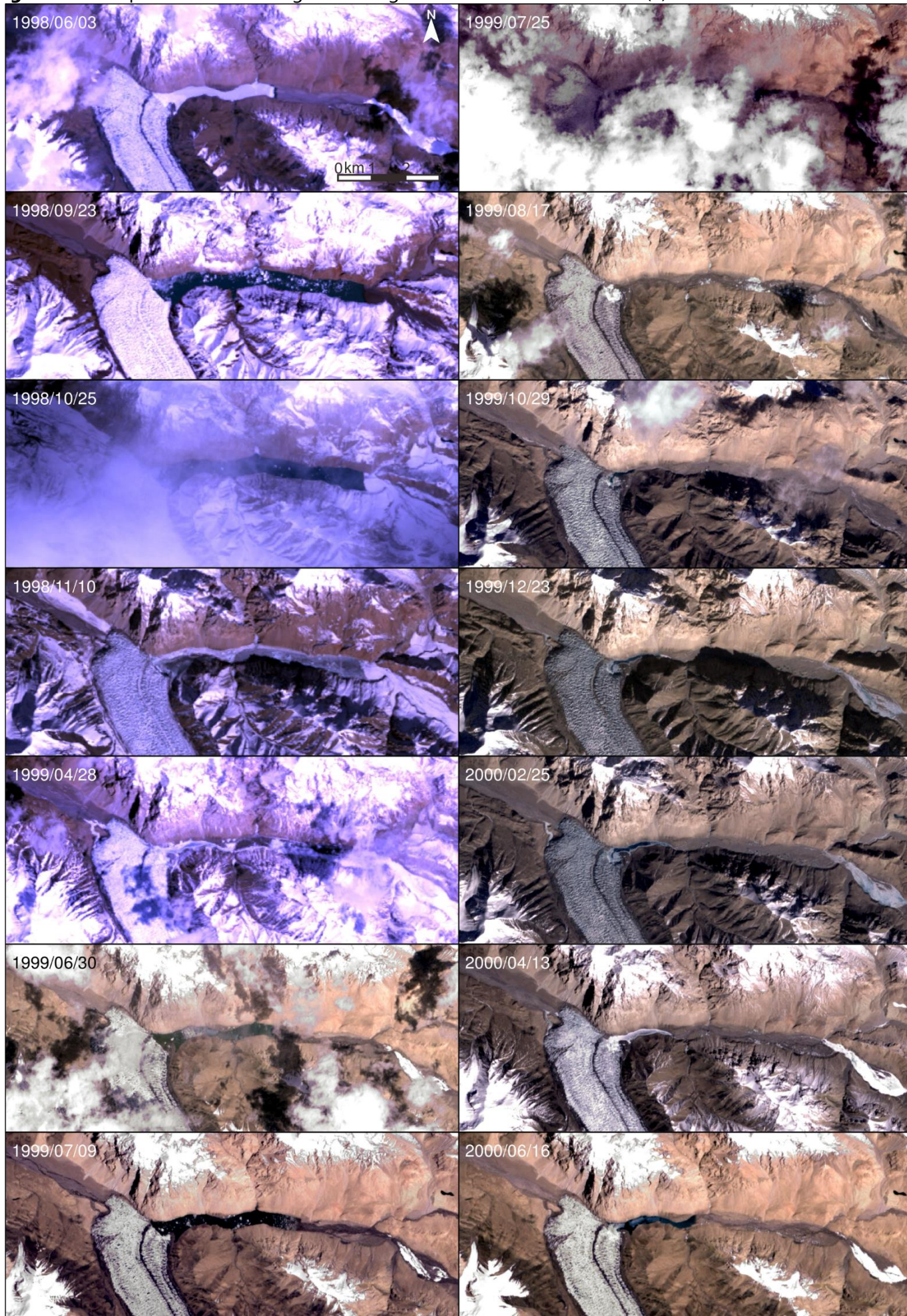


**Figure S3.** Sharpened Landsat images showing ice-dammed lake evolution (3).

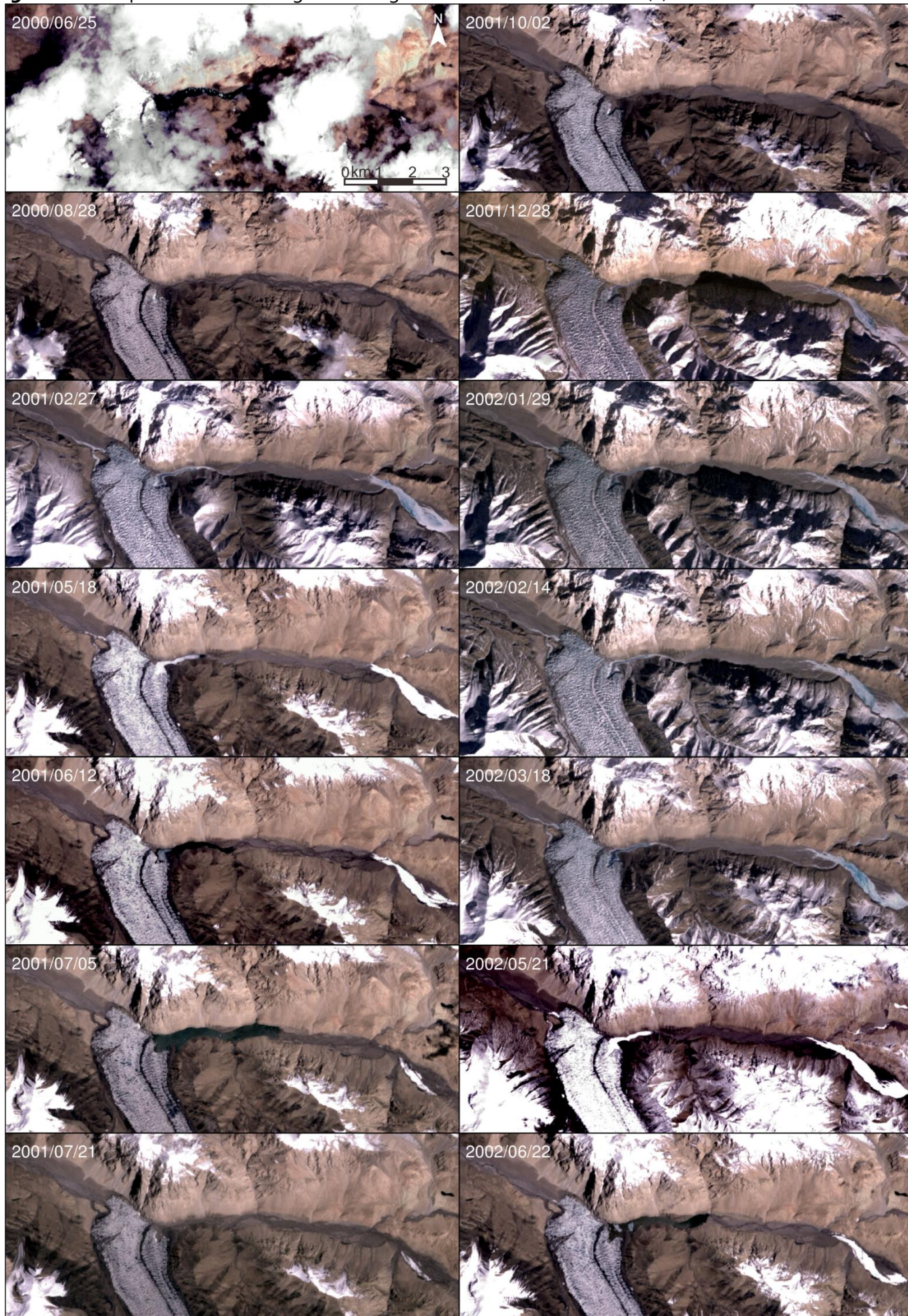


**Figure S4.** Sharpened Landsat images showing ice-dammed lake evolution (4).



**Figure S5.** Sharpened Landsat images showing ice-dammed lake evolution (5).

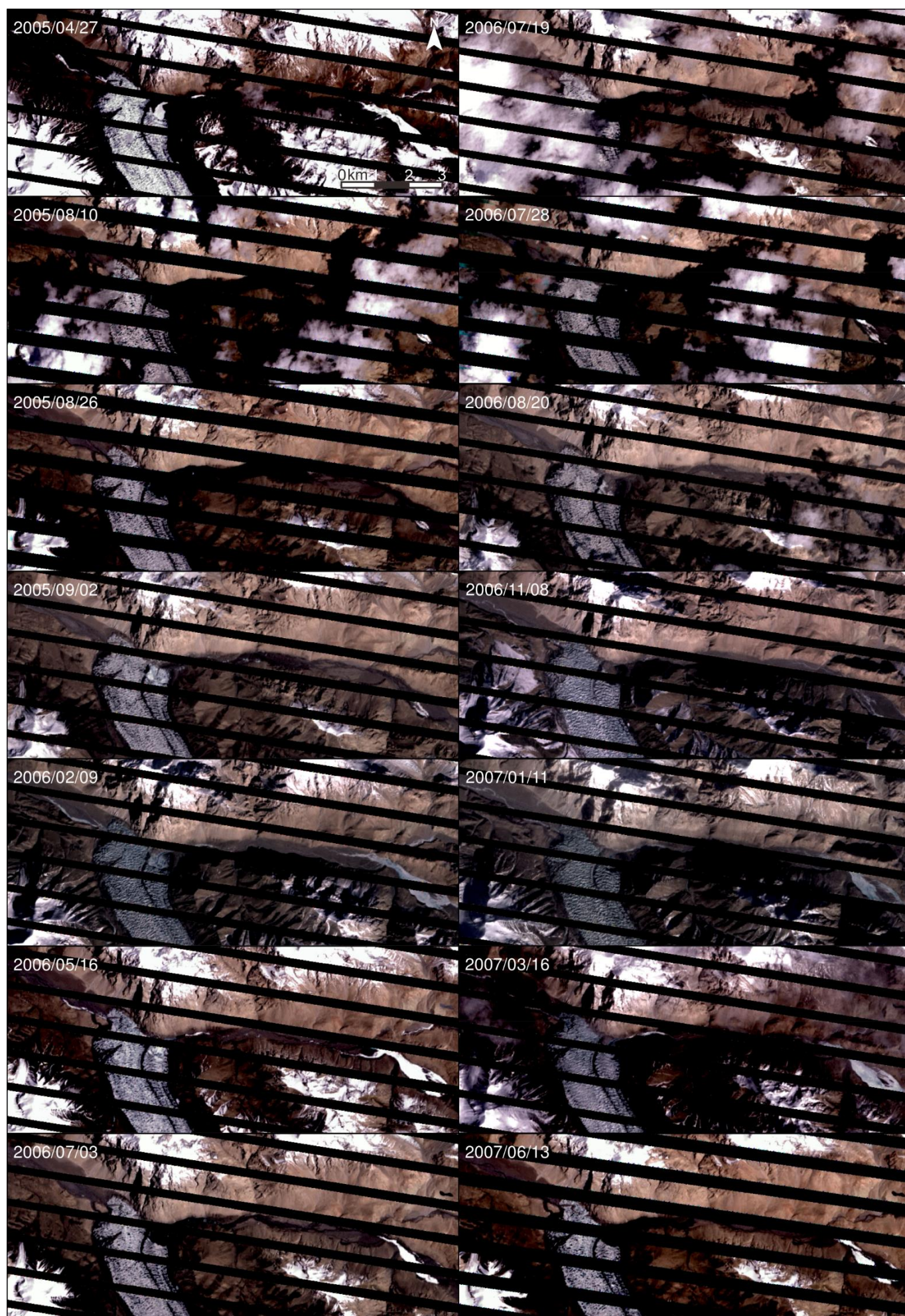


**Figure S6.** Sharpened Landsat images showing ice-dammed lake evolution (6).

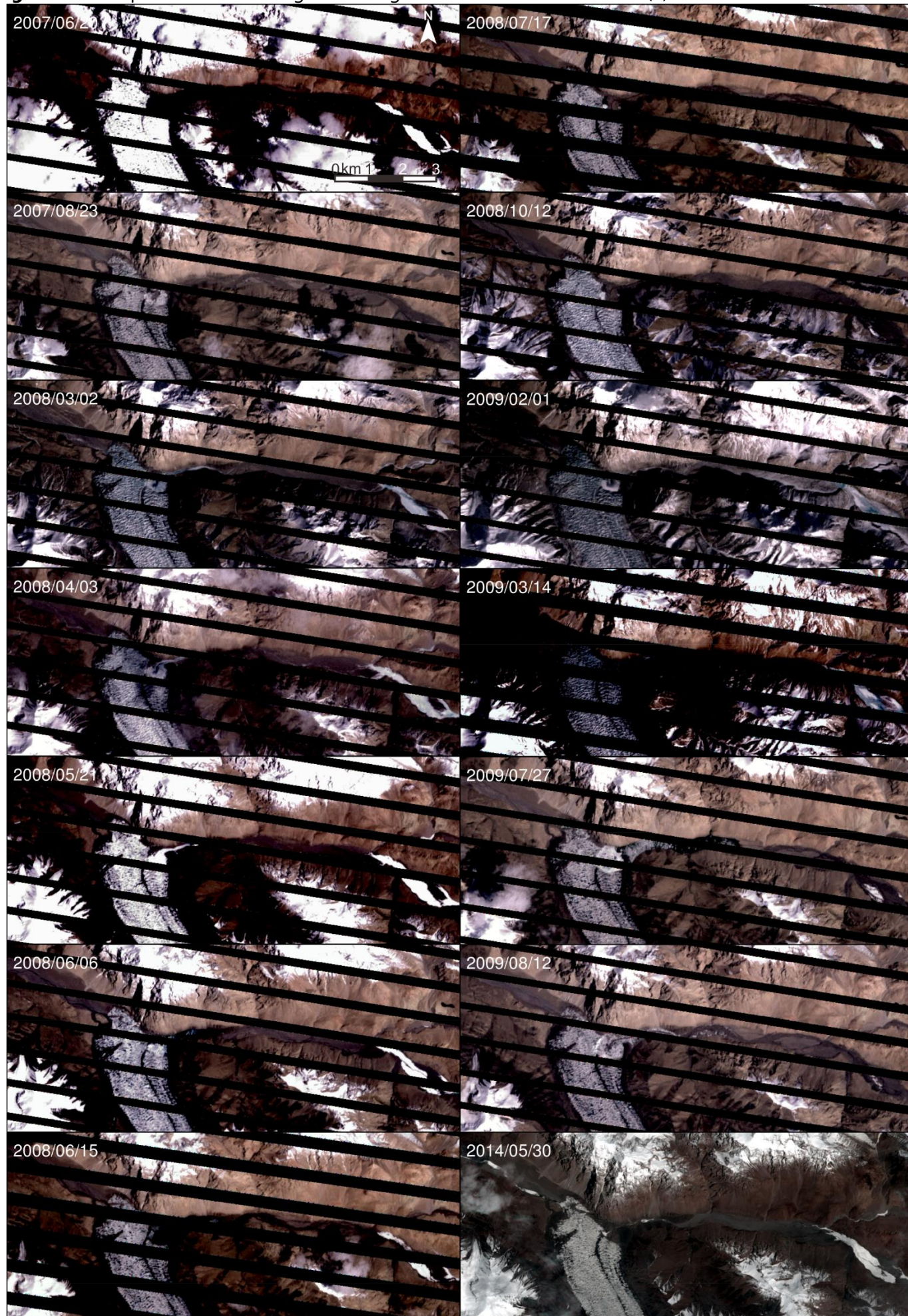


**Figure S7.** Sharpened Landsat images showing ice-dammed lake evolution (7).

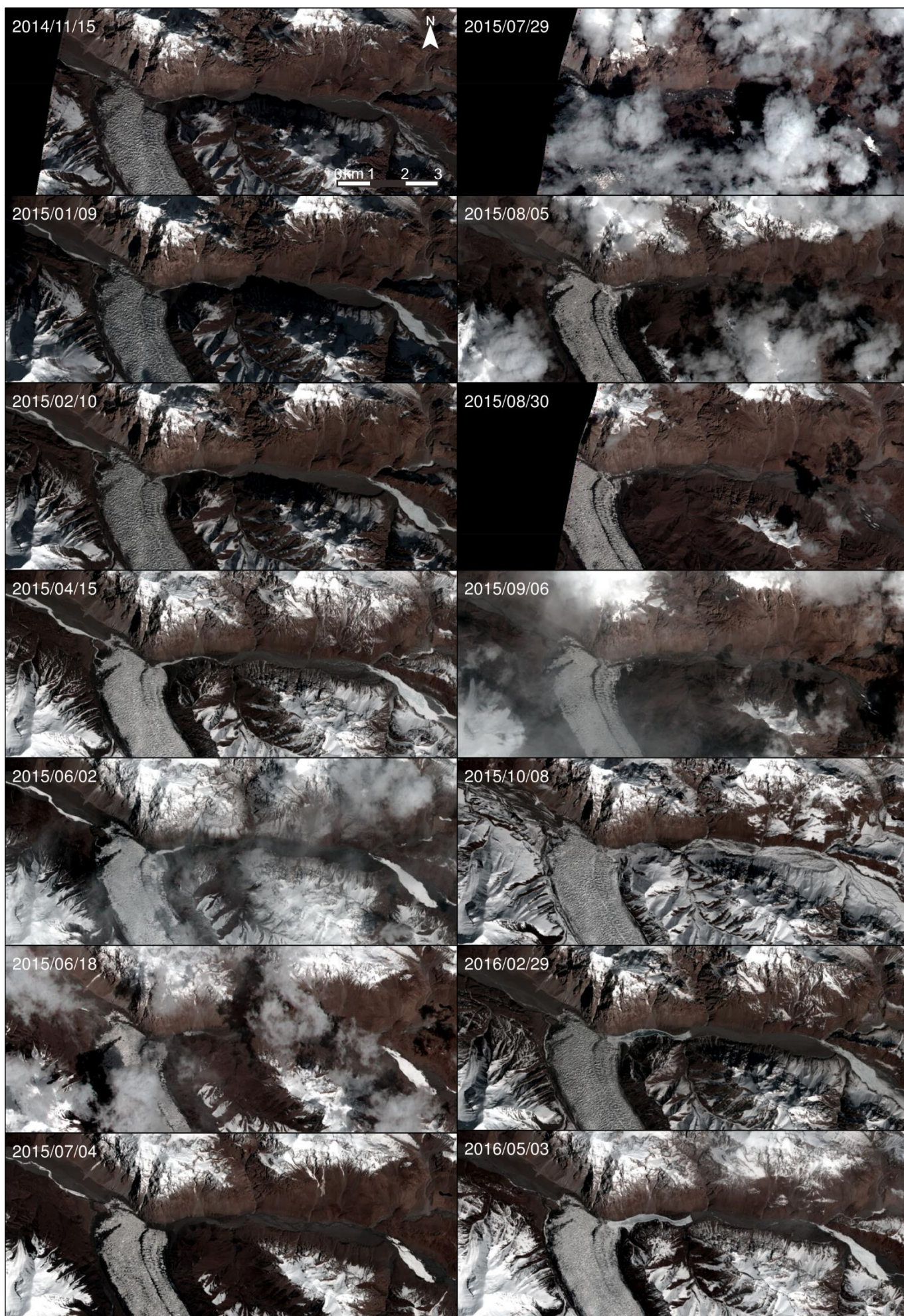


**Figure S8.** Sharpened Landsat images showing ice-dammed lake evolution (8).

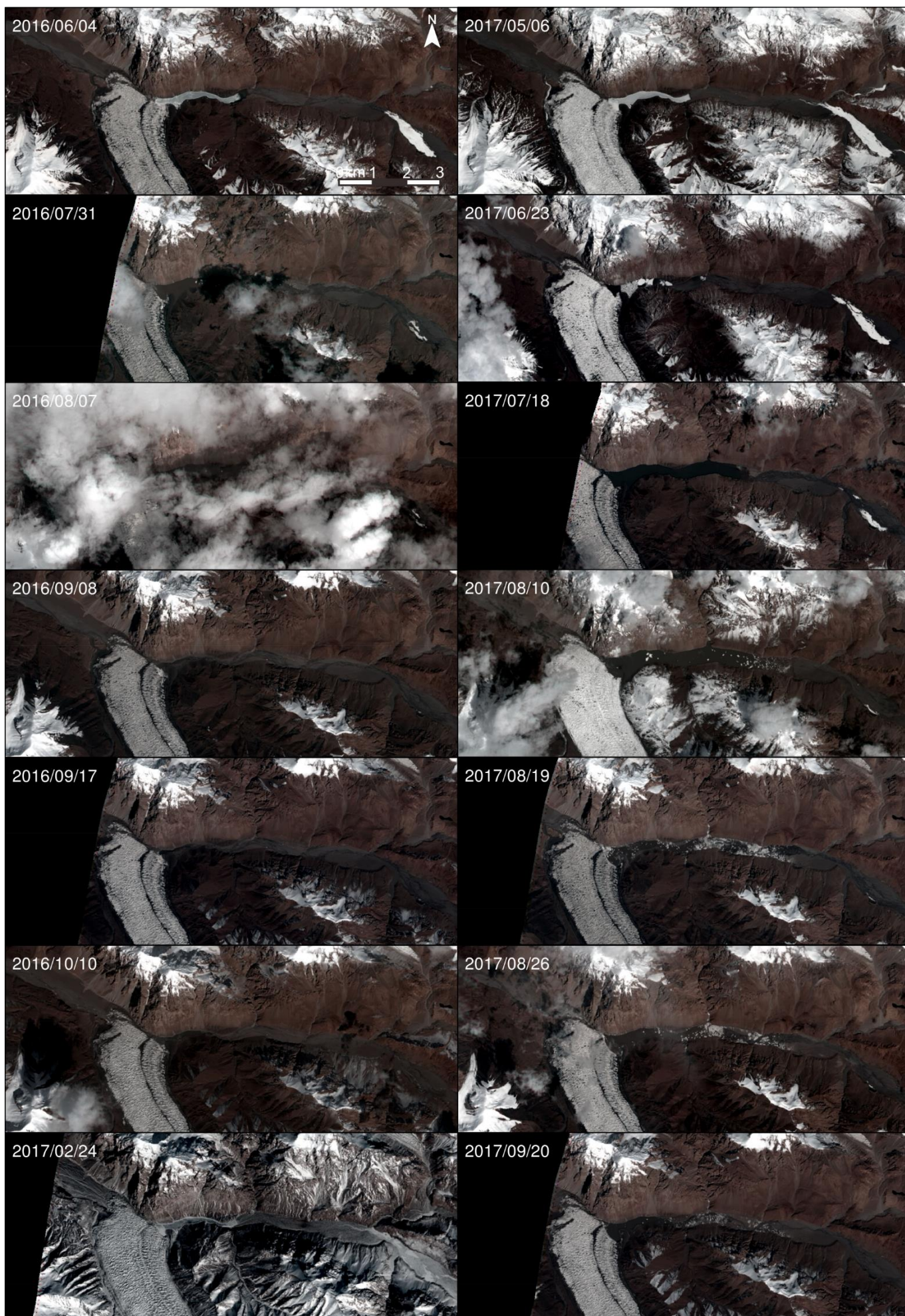


**Figure S9.** Sharpened Landsat images showing ice-dammed lake evolution (9).

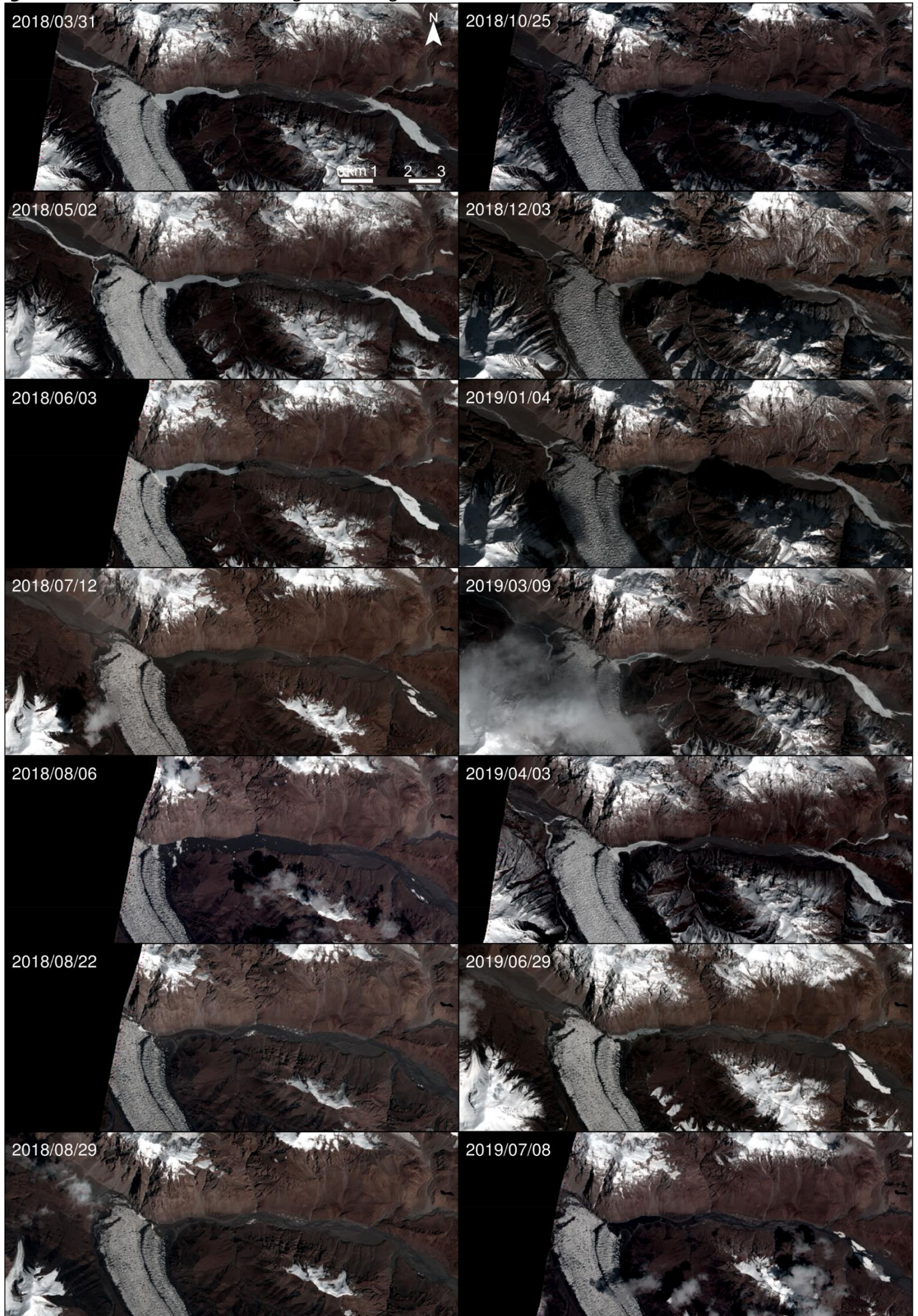


**Figure S10.** Sharpened Landsat images showing ice-dammed lake evolution (10).

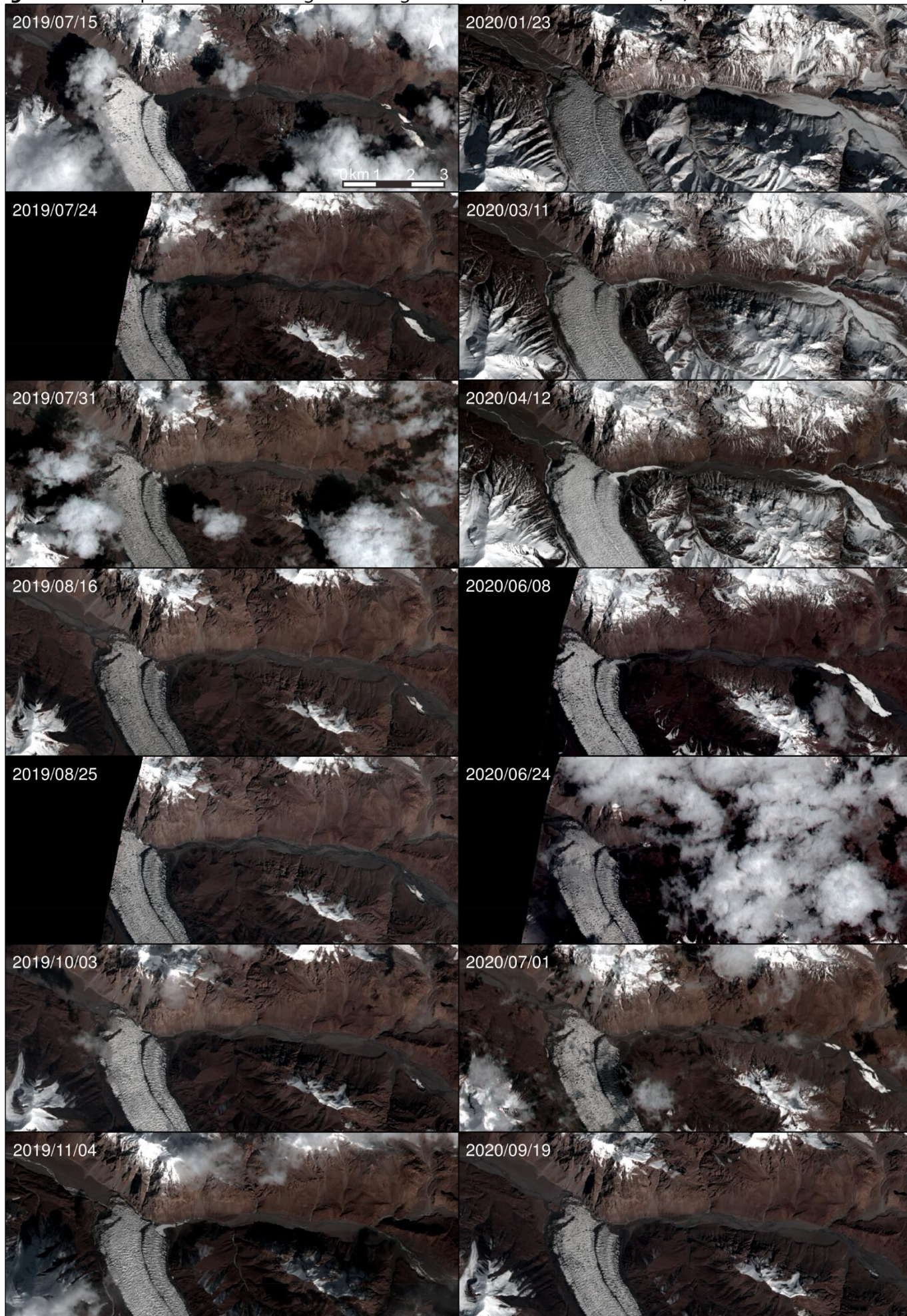


**Figure S11.** Sharpened Landsat images showing ice-dammed lake evolution (11).

